IMAGE: A MAP OF THE STARS OF THE ORION CONSTELLATION

Print ISSN: 2631-8474 Online ISSN: 2631-8482

JournalPreview

London Journal of Engineering Research

Volume 22 | Issue 5 | Compilation 1.0

London Journals Press

WWW.JOURNALSPRESS.COM
© COPYRIGHT LONDON JOURNALS PRESS

JournalPreview

LONDON JOURNAL ENGINEERING RESEARCH

This document is a pre-published view of London Journal of Engineering Research Volume 22, Issue 5 and Compilation 1.0. For any minor changes and updations kindly follow your paper's live editing URL given in sent email or get in touch with our support team at support@journalspress.com or visit our website to use live chat support. This is a beta document thus order, content or existence of papers may alter in the published eJournal. You are requested to kindly acknowledge and approve your research paper in this JounalPreview within three days.

*THIS IS A CONFIDENTIAL DOCUMENT UNDER A SOLE COPYRIGHT OF LONDON JOURNALS PRESS. IT IS STRICTLY PROHIBITED TO SHARE THIS DOCUMENT OR ITS COPY IN ANY FORMAT WITH OTHERS OR IN PUBLIC WITHOUT PRIOR PERMISSION OF LONDON JOURNALS

Journal Content
In this Issue

London Journals Press

©2022 London Journals Press

Scan to know paper details and
author's profile

Experimental Study of Vibrations of Cross-Rod Spatial Structures

Khalmuradov R.I., Khudoynazarov K. & Isabekov K.

Samarkand State University

ABSTRACT

This article explores a technique for studying the dynamic characteristics of cross-rod spatial structures (CRSS) using small-scale models, including the developed nodal connection of spatial frame rods, protected by copyright. The use of a nodal connection makes it possible to regulate the construction lifting of large-span structures, increases their strength and reliability. The developed nodal connection of the structure can be used for any spatial frames of buildings and structures and is especially effective for the frames of buildings erected in areas of high seismicity.

The issue of choosing methods for excitation of free and forced vibrations is being investigated, equipment for recording and recording vibrations is selected, and a layout of vibration sensors and sources of excitation of free and forced vibrations is being developed. Natural vertical oscillations of the structure model were caused by removing it from the state of equilibrium by concentrated loads applied in the middle and in a quarter of the span with their subsequent removal.

Keywords: NA

Classification: DDC Code: 572.86 LCC Code: QH450.2

Language: English

London Journals Press

LJP Copyright ID: 392911
Print ISSN: 2631-8474
Online ISSN: 2631-8482

London Journal of Engineering Research

Volume 22 | Issue 5 | Compilation 1.0

© 2022. Khalmuradov R.I., Khudoynazarov K. & Isabekov K. This is a research/review paper, distributed under the terms of the Creative Commons Attribution-Noncom-mercial 4.0 Unported License http://creativecommons.org/licenses/by-nc/4.0/), permitting all non-commercial use, distribution, and reproduction in any medium, provided the original work is properly cited.

Experimental Study of Vibrations of Cross-Rod Spatial Structures

Khalmuradov R.I.[α], Khudoynazarov K.[σ] & Isabekov K.[ρ]

ABSTRACT

This article explores a technique for studying the dynamic characteristics of cross-rod spatial structures (CRSS) using small-scale models, including the developed nodal connection of spatial frame rods, protected by copyright. The use of a nodal connection makes it possible to regulate the construction lifting of large-span structures, increases their strength and reliability. The developed nodal connection of the structure can be used for any spatial frames of buildings and structures and is especially effective for the frames of buildings erected in areas of high seismicity.

The issue of choosing methods for excitation of free and forced vibrations is being investigated, equipment for recording and recording vibrations is selected, and a layout of vibration sensors and sources of excitation of free and forced vibrations is being developed. Natural vertical oscillations of the structure model were caused by removing it from the state of equilibrium by concentrated loads applied in the middle and in a quarter of the span with their subsequent removal.

The test results and their analysis are analyzed. The elements of experimental models at all stages of loading worked in the elastic stage. The tests carried out showed that the structure has sufficient strength, stability, rigidity and seismic resistance. On the basis of the results obtained, recommendations were made for their use in the calculation and design of CRSS for seismic regions.

Author α σ ρ: Doctor of Technical Sciences, Professor of department of Theoretical and Applied Mechanics, of Samarkand State University.

I. INTRODUCTION

Due to the variety of seismic actions and the specific features of the CRSS, the range of problems associated with their oscillations and dynamic calculation is very wide. From a seismic point of view, PSPKs are systems with distributed parameters and an infinite number of degrees of freedom. Vibrations of spatial structures are of a complex nature and are determined by the joint spatial displacements of nodes and rod elements of the CRSS [1].

The analysis of literary sources also showed that there is a significant discrepancy between the experimental and theoretical results obtained in the process of experimental studies on full-scale structures [2, 3, 4].

Therefore, despite the successes, in general, the problem of seismic resistance of the CRSS has not been resolved. To solve it, further theoretical and experimental studies are required. Carrying out full-scale studies of the seismic resistance of FPCS, especially with various design schemes, seems to be very laborious and expensive. Based on this, in this article an attempt is made to solve these problems in a more accessible way with the help of experimental studies on small-scale models. In this article, we study a technique for studying the dynamic characteristics of CRSS using small-scale models, including a newly developed nodal connection of rods of a spatial frame, protected by an author's certificate [5].

© 2022 London Journals Press

II. METHOD

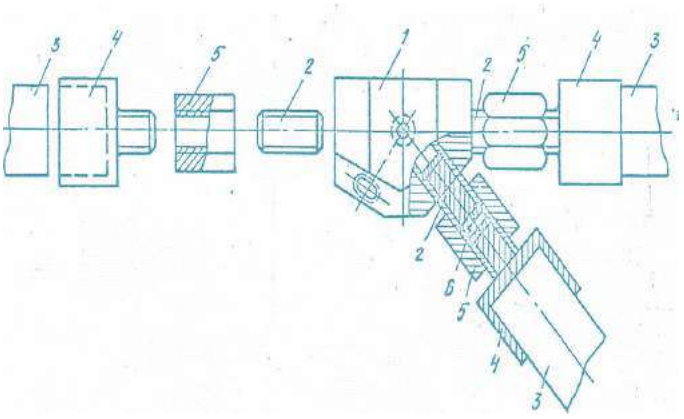

Fig. 1: Nodal Connection of the Rods of the Spatial Frame

2.1 Description of the Nodal Connection of the CRSS

The experimentally investigated nodal connection contains a nodal element 1 of a spatial frame with studs 2 freely fixed in it, to which rods 3 with rigidly fixed tips 4 are attached by means of a moving coupling 5 with a gap. The connection of the rod 3 with the nodal element 1 is carried out by moving the coupling 5 from the pin 2 to the threaded part of the tip 4, while the length of the rod in the axes of the nodal elements is regulated by the gap 6 between the pin and the tip, and the preliminary the tension is achieved by the depth of screwing the pin 2 into the threaded hole of the nodal element. The use of a nodal connection makes it possible to regulate the construction lifting of large-span structures, increases their strength and reliability. The developed nodal connection of the structure can be used for any spatial frames of buildings and structures and is especially effective for the frames of buildings erected in areas of high seismicity.

2.2 Creation of a Model Structure

New structures intended for construction in seismic areas are investigated not only for the effects of seismic loads, but also for the effects of conventional static loads.

In addition, the method for calculating structures for seismic regions adopted by the current standards assumes that after determining the seismic loads, the latter are applied statically to the structures. In experimental studies of CRSS, sometimes the dynamic load is replaced by a static one in order to identify, as a first approximation, the general nature and features of the stress-strain state of CRSS. Thus, static studies of structures for seismic regions are, on the one hand, of independent importance, and on the other hand, they serve as a kind of model for the work of the CRSS on seismic effects.

Taking into account the specifics of the impact on the structure of harmonic vibrations, which depend on external factors and, in particular, on the material of the model, for model imitation of metal rod structures, it was decided to make a model from metal rod and node elements.

The prerequisites underlying the constructive solution of the experimental model were the following:

- geometric similarity between the model and the real structure, achieved by the ratio of the lengths of the rods equal to 1/10;
- the similarity of the rigidity of the rods of the model and the real design achieved by using tubular rods of various diameters of 6.8 and 12 mm;
- the similarity of the nodal connection in the model and the real structure, achieved by using a single bolted connection, working on longitudinal tensile-compression forces.

Tests of the structure model for a static load were carried out in order to establish a qualitative and

© 2022 London Journals Press

quantitative coincidence of the results of the actual stress-strain state with the results of an accurate calculation performed on a computer [6, 7].

During the experiment, the ambient air temperature was constant, which made it possible to measure vibrations of any direction with the same sensor (horizontal or vertical). The tests were carried out to make a decision on the possibility of using the experimental model for dynamic testing.

Oscillations of the structure model, both in the vertical and horizontal directions, were excited:

- instant removal of suspended loads;
- guying of the column heads with the calculated static load when it is instantly released;
- falling load;
- vibration motor, on the shaft, which was mounted with eccentrics.

Natural vertical oscillations of the structure model were caused by removing it from the state of equilibrium by concentrated loads applied in the middle and in a quarter of the span with their subsequent removal. The natural horizontal oscillations of the structure model were caused by a static load pulling the top of the columns with its instantaneous release. The load was released and the columns were pulled using a system of cables, and the mass of the load was 10–15% of the mass of the structure model under study.

The maximum number of revolutions developed by the vibrating machine used was 1800 revolutions per minute, which corresponded to the highest frequency of forced vibrations of the PSPK 30 Hz. At the maximum number of revolutions, the amplitude of the load created was 90 N. The eccentric load had a mass of 100 g. and fastened at a distance of 2.5 from the axis of rotation. The number of revolutions of the vibrator (the frequency of the studied oscillations) was regulated using an autotransformer introduced into the installation circuit of the vibrator. In this case, the inertial force was determined by the well-known formula:

$$P = 4\pi^2 m_{эl э}\ \omega^2$$

Where $m_э$ is the mass of the eccentrics; $l_э$ is the eccentricity equal to 2.5 sm; ω - is the number of revolutions in 1 second. Note that the magnitude of the inertial force of the vibrating machine was chosen in such a way as to cause oscillations with amplitudes that could be recorded by an oscilloscope with sufficiently large magnifications and at the same time not cause nonlinear oscillations [8].

2.3 The Choice of Equipment

The choice of equipment for recording vibrations was made taking into account the possibility of recording waveforms in the frequency range from two to 30 Hz, and amplitudes from 1 to 100 microns and obtaining multipoint recording in movements to identify possible forms of vibrations. The following equipment was used during the tests:

1. A set of devices for measuring vibration of type K001, consisting of horizontal vibration sensors of type I001G, vertical vibration sensors of type I001B, a magnification regulator R001, integrating galvanometers of type M002 and a 14-channel light-beam oscilloscope of type POB-14. The frequency measurement range for the kit K 001 was 1.5-200 Hz. The permissible oscillation amplitude is up to 1000 microns.
2. Miniature seismic receivers SMV-30 of the "Firefly" type, used to control some experiments that exclude the influence of the mass of vibration sensors K001. They are converters of mechanical movements into electrical signals and are designed to register the vertical components of seismic waves. The range of measured frequencies is from 1 to 300 Hz, and the natural frequency of the device is 29 = 1 Hz, the diameter of the device is 29 mm, the length with a tip is 100 mm, the weight of the device without a tip is 100g.
3. In some rods of the design model, deformations were recorded by strain gauges with recording on the POB-14 oscilloscope via the V-ANCH-7M amplifier.

© 2022 London Journals Press

The square shape of the experimental models determined the installation location of the vibration sensors along the axes of the quarter, and the vibration machines in the center of the structure and the quarters of the spans.

Micro-vibrations of the base were excluded by the massiveness of the experimental stand and were controlled by a vibration sensor. By pre-installing the vibration sensors on the model, they were calibrated to determine the frequency and amplitude characteristics and to adjust the same phase of the vibration sensors necessary to determine the waveforms.

Vertical vibration sensors were installed on special round plates using 4 M6 bolts, and horizontal vibration sensors were installed on special angles using 4 M-6 bolts.

2.4 Calibration of a Set of Devices

Calibration of the set of instruments was carried out as follows:

1. Vibration sensors were installed on special calibrated stands that create vibration with the required frequency and amplitude. The vibration stand platform produced harmonic vibrations. The control of the frequency and amplitude of the oscillations was carried out with greater accuracy than the control of the tested devices.
2. Galvanometers used in conjunction with a set of instruments were installed in certain channels of the oscilloscope, and when measuring vibrations, galvanometers were installed, and the same channels of the oscilloscope.
3. The frequency and amplitude characteristics in the operating range of frequencies and amplitudes were removed, the values of the magnification coefficients were determined. Dynamic tests began with the installation of minimal eccentric loads on the vibrating machine and the creation of vibrations with a slow increase and decrease in the speed of the electric motor, regulated by an autotransformer in the frequency range from 1 to 30 Hz.

By visual observation on the oscilloscope screen, the resonant oscillation zones were determined and the recording scale and the speed of the photo paper were determined. In the zone of resonant revolutions of the fundamental tone, the attenuation of free vibrations was studied when the vibrating machine was switched off. Only mechanical devices were installed to measure vertical movements along the lower belt of the model. By changing the place of application of force or load (the source of excitation of free and forced oscillations), the nature of changes in dynamic parameters was established [9].

The frequency of free oscillations was determined both by the oscillograms of damped free and forced oscillations, and by the diagrams of resonant curves[10]. The values of the logarithmic decrement were determined by damped free oscillations, as well as by resonant curves [11].According to the amplitudes recorded simultaneously at 6 points, plots representing waveforms were constructed.

2.5 Determination of Dynamic Characteristics

The tests were carried out to identify the stress-strain state and dynamic parameters (periods, shapes, and decrement fluctuations) of the CRSS with various support options and structural schemes and to establish the influence of enclosing structures on the stress-strain state and dynamic characteristics. All waveforms recorded during dynamic tests were processed according to a single methodology. At each level of free oscillations, the most characteristic and stable section was selected, on which the dynamic parameters of the design model were determined. According to these values, taking into account the calibration data of the equipment, the movements of individual points of the model were determined, which made it possible to identify the forms of its oscillations.

The oscillograms represented a picture of oscillatory motion expanded in time. They were used to determine the frequencies and periods of oscillations, as well as the amplitudes of oscillations. To determine the oscillation amplitudes on an oscillogram, the distance

© 2022 London Journals Press

between adjacent half-wave vertices was measured. Half of this distance is the amplitude. For the accuracy of determining the amplitude, the scale of recording the waveforms was of great importance, therefore, the maximum magnification of the regulator was used. When determining the oscillation period, the first two half-waves of the oscillogram were not taken into account, since they were influenced by various transients.

The rest of the waveform obeyed a general pattern and the oscillation periods were determined by it. On the oscillogram, the natural oscillation period of the structures is 0.2 and 0.16 s, respectively, hence the oscillation frequencies f = 1 / T turned out to be equal to 5 Hz and 6 Hz, respectively.

Recordings of free damped oscillations made by:

- at different stages and with different types of loads of the structure with a constant load and with different support options;
- various design schemes;
- various levels of dynamic stresses characterized by the magnitude of the broken load allowed us to obtain numerical values of the logarithmic decrement.

According to the recording of the oscillogram, the ratio of adjacent amplitudes and periods was found, the vibration attenuation coefficient K3 was determined.

$$K_3 = \delta / T$$

Where, δ is the natural logarithm of the ratio of adjacent amplitudes, called the logarithmic decrement of oscillations.T is the period of free oscillations.

The value of the coefficient for metal structures is usually recommended to be taken depending on the level of dynamic stresses at low loads of 0.01, and at high loads - 0.025. The amplitudes of movements in the center of the PSPC served as a generalized characteristic of the level of dynamic stresses of the structure, since the fluctuations of the PSPC during the breakage of the load occurred in the first form.

III. RESULTS AND DISCUSSIONS

According to the results of processing vibrograms of their own damped oscillations, the dependences of γ(a) of the loss coefficient on the amplitude of the oscillations (in the first form) in the center of the plate were found. According to the obtained oscillograms, the first 3 forms of natural vibrations of the structure were constructed. The amplitude - frequency characteristics of oscillations for individual points were also constructed. The frequencies, shapes and amplitudes of the natural oscillations of the unloaded model were also determined, as well as at a loading stage of 20% of the calculated one. Then a vibration motor was installed and forced vibrations were created at various stages of loading.

At the same time, the experimental results (the frequency and amplitude of the natural oscillations of the model) corresponding to different stages of loading with a constant load, in the presence of loads differ from each other by more than 20%, and the frequencies in the presence of loads are greater than in the absence of it.

This is due to the fact that loading practically does not affect the rigidity of the model. Loading caused an increase in mass, which, in turn, caused an increase in the values of the period of natural oscillations. Experimental studies show that with low-mass eccentrics, changes in frequencies and decrements of vibrations both at the beginning of the vibration machine and after some time of operation of the vibration machine occur slightly, only amplitudes increase.

With eccentrics of a larger mass, the oscillation frequencies noticeably decrease and the amplitudes and decrements of oscillations significantly increase. According to the results of processing the oscillograms of their own damped oscillations, the dependences of the loss coefficient γ(a) were foundfrom the amplitude of the oscillations in the center of the CRSS model. The arrangement of the curves in Fig.2 indicates that with increasing static stresses in the structure, the value of the inelastic resistance coefficient decreases.

© 2022 London Journals Press

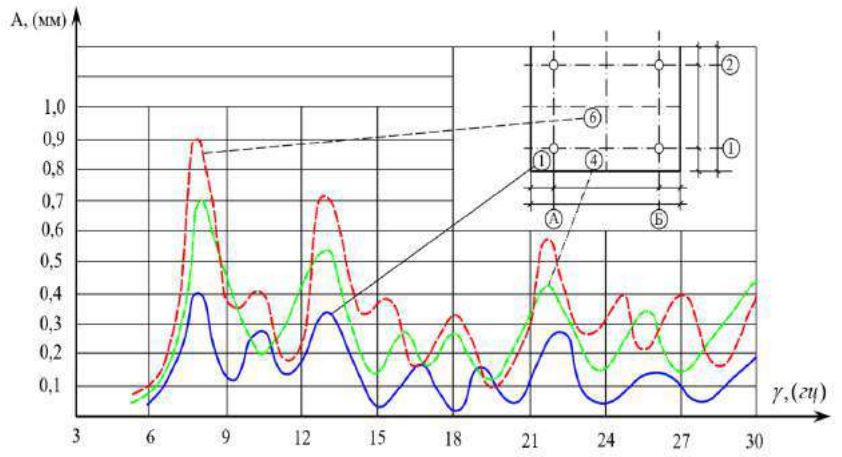

Fig. 2: Resonant Curves of Forced Oscillations of Various Nodal Points

It has been experimentally established that the coefficient γ at a low level of dynamic stresses can take a value less than that accepted in regulatory documents.It is characteristic that at a low level of dynamic stresses, the value of the loss coefficient (γ = 0.0065) for PSPC is 35% less than that accepted in regulatory documents.At the maximum level of dynamic stresses, the value of γ is equal to 0.018 for the same type of structures, which is 20% less than accepted in regulatory documents.This fact has a noun meaning, since we are talking about calculations of oscillations of repeatedly statically indeterminate systems in the resonant mode [12,13]. The results of tests for vertical seismic loads showed that 3 resonant zones were recorded on the oscillogram for the PSPC models with a smooth decrease in often forced vertical oscillations. With the growth of external uniformly distributed static and dynamic loads, there was a decrease in the frequencies of natural vertical vibrations and the dynamic stiffness of the PSPC, and their shapes did not change [14].

This is typical for systems in which the dissipation of oscillation energy is caused by an internal inelastic resistance [15,16]. Under the action of a horizontal load, a coating with columns in the first approximation can be considered as a system with one degree of freedom or with an infinite number of degrees of freedom. For example, for a system with one degree of freedom, comparing the values of frequencies can cancel the proximity of their values.

At all stages of loading, the structure worked elastically, without residual deformations after unloading. The forces in the rods increased in proportion to the increase in the inertial impact and the design load in the range up to 2700 Pa.From the evenly distributed load over the entire coating, the struts of the structure along the main diagonal were the most loaded. Under seismic impacts, the forces in these struts increased from 5 to 18%. The greatest tensile force from the 9-point seismic load was recorded in the rod of the upper belt above the support, the greatest compressive force from the 9-point seismic load was in the struts of the support zone.

As can be seen from Fig.3. When the constant load q = 1080 Pa and 2700 Pa, the graphs γ(a) have a horizontal increase in amplitudes and a sharp decrease in the values of γ in the regions of small amplitudes. In the center of the structure, the greatest force in the rods reached 825N. The greatest effort was in the rod directed towards the center of the structure along the main diagonal of the support pyramid. In the rods forming the base of the support pyramid and located above the braces, the forces are small-163 N.

© 2022 London Journals Press

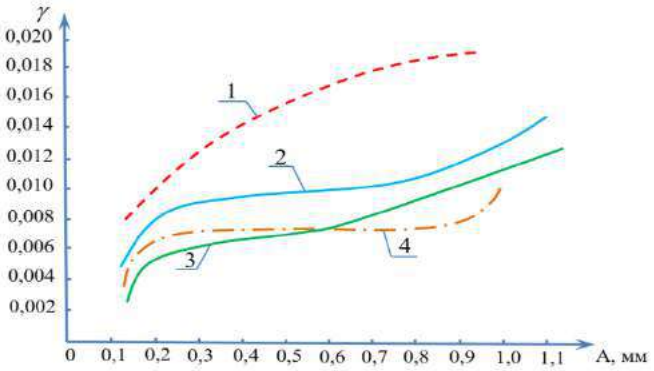

Fig. 3: Dependence γ(A) for Different Levels of Loading of the Model With a Constant Load: 1,2,3,4 - at a Load of 0.54; 1.08; 1.68; 2.7 kN/m2.

With the growth of the external uniformly distributed load and dynamic loads, there is a decrease in the frequencies of natural vertical vibrations and the dynamic stiffness of the PSPC while maintaining their constant shape.

The results of tests for vertical loads of the seismic type showed that the CRSS model, with a smooth decrease in the frequencies of forced vertical oscillations, three resonant zones are fixed on the oscillogram.

Experiments have also shown that the periods of proper vertical oscillations of experimental models are in the range of 0.06 - 0.207 sv depending on the type of models and the conditions of support. The nature of the variation in the oscillation amplitudes of individual points of the CRSS was revealed, gradually fading in time, and logarithmic decrements were determined for vertical oscillations, the value of which is not less than 0.09.

IV. CONCLUSION

The results of testing experimental models have shown that under the action of a horizontal load, the PSPC together with the columns can be considered as a system with one degree of freedom in the first approximation or as a system with an infinite number of degrees of freedom.

Comparison of the frequency values obtained theoretically in accordance with the recommendations of building codes and regulations for systems with one degree of freedom with the results of experimental studies showed that these values practically coincide (respectively equal to 12.5 and 11.8 Hz.

The periods of horizontal natural oscillations of the PSPC were in the range of 0.03 - 0.147 s, and the logarithmic decrements of the oscillations did not exceed 0.04. From the evenly distributed load over the entire coating, the struts in the support zone of the structure were the most loaded. The increase in the forces in the core elements of the structure, taking into account the vertical seismic load, amounted to a maximum of 18% for the model with a plan size of 3.0 x 3.0 m, and 14% for the 3.6 x 3.6 m model. The elements of the experimental models at all stages of loading worked in the elastic stage.

The nature of the deflections of the model corresponded to its tense state. The greatest deflection under normal symmetrical load was fixed in the middle of the model and is equal to 5.23 mm, which was 1/425 of the span and indicated sufficient rigidity of the model structure.

A comparison of the experimental data obtained with the results of calculations using the displacement method using finite elements showed their fairly good correspondence. The experimental data exceeded the calculated ones by only 12-19%. The tests have shown that the structure has sufficient strength, stability, rigidity and earthquake resistance. Based on the results obtained, recommendations are made for their use in the calculation and design of PSPCS for seismic areas [17].

© 2022 London Journals Press

REFERENCES

1. Isabekov K. Experimental studies of cross-rod spatial structures on small-scale models.., Samarkand: 2021. Navruz Polygraph. 121 p.
2. Abdurashidov K.S. In the collection "Effective spatial structures in the practice of design and construction of the Republics of Central Asia and Kazakhstan". G. Frunze, 1989. Pp.102-106.
3. Ivanov M.N., MironovE.M., Mixylov G.G., Platov G. S. In the collection. "The use of aluminum alloy structures in high-speed construction of industrial and civil buildings." Moscow: Metallurgy. 1988.pp. 77-102.
4. Bolotin V.V., Radin V.P., Cyirkov V.P. Modeling of dynamic processes in elements of building structures during earthquakes.News of universities. Construction. Moscow: 1999. pp122- 129.
5. Isabekov K. SSSR. Patent No. 885478. (22 July 1981).
6. Ibragimov N. X., Isabekov K. To the choice of a mathematical model of rod systems of the truss type. “Promlems of architecture and construction” (scientific and technical journal). Samark and .2021.No.2.pp.121-125.
7. Sventikov A.A.Computational Civil and Structural Engineering, Volume 4, Issue 2, 2008.pp83-88.
8. Khalmuradov R.I., Khudoynazarov Kh., Khudoyberdiyeva S. Uzbekistan Problems of Mechanics, No.2-3, 2017, pp. 46-52.
9. KhalmuradovR.I Scientific Bulletin of Samarkand State University, No.3, 2017, pp.86-90.
10. Isabekov K. Middle European Scientific Volume - 18 (2021) .221-224.November ISSN (E): 2694-9970
11. Khalmuradov R.I., Khudoynazarov K., Nishonov U.A. Int. Journal of Advanced Research in Science, Engineering and Technology. Vol. 5, Issure 3, March 2018. – pp. 5289-5296.
12. Khudoynazarov Kh. Kh., Khalmuradov R.I., Yalgashev B.F. 2021 Tomsk State University. Journal of Mathematics and Mechanics. 69, 139-154. DOI: 10.17223/19988621/69/11
13. Khudoynazarov Kh., Khudoyberdiyev Z. Khudoyberdiyeva S. Int. J. of Advanced Research in Science, Engineering and Technology, 2018. Vol.5, Issue 10.-pp.7117-7121.
14. Raximov A.K. European Scholar Journal (ESJ)Available Online Vol. 2 No.12, 277-281. December 2021 ISSN: 2660-5562.
15. Khudoynazarov Kh., Yalgashev B.F.and T.Mavlonov 2021.IOP Conf. Series: Mater. Sci. Eng.1030012098 DOI:10.1088/1757-899X/1030/1/012098.
16. Filippov, I. G. Kudainazarov, K. (1998). International Applied Mechanics, 34(12), 1204–1210.
17. Guidelines for the design of structural structures. Moscow: Stroyizdat. 1984. pp.258-274.

© 2022 London Journals Press

Scan to know paper details and
author's profile

Omicronvirus Data Analytics using Deep Learning Technique

Mr. Anand Kumar Gupta, Dr. Asadi Srinivasulu, Dr. Kamal Kant Hiran, Dr. Tarkeswar Barua, Mr. Goddindla Sreenivasulu, Dr. Sivaram Rajeyyagari & Dr. Madhusudhana Subramanyam

BlueCrest University

ABSTRACT

The Man-made brainpower (AI) methods overall and convolutional brain organizations (CNNs) specifically have achieved victories in clinical picture examination and grouping. A profound CNN design partakes projected into this research article for the analysis of OMICRON grounded onto clinical radiography analysis (X-ray). As matter of fact the non-availability in adequate scope and excellent X-ray picture database, a compelling & exact Convolutional NN (CNN) characterization remained an examination. Managing those intricacies, for example, accessibility with a very-little measured and contrast database of picture resolution challenges, the database has pre-processed been into various stages utilizing various strategies to accomplish a powerful preparation database of the applied Convolutional NN (CNN) prototypical to achieve its finest presentation.

Keywords: omicron disease, cross-validation methods, classification algorithms, disease prediction, CNN, data minelaying, feature selection, data pre-processing.

Classification: DDC Code: 171.2 LCC Code: PA6308.D5

Language: English

London Journals Press

LJP Copyright ID: 392912
Print ISSN: 2631-8474
Online ISSN: 2631-8482

London Journal of Engineering Research

Volume 22 | Issue 5 | Compilation 1.0

© 2022. Mr. Anand Kumar Gupta, Dr. Asadi Srinivasulu, Dr. Kamal Kant Hiran, Dr. Tarkeswar Barua, Mr. Goddindla Sreenivasulu, Dr. Sivaram Rajeyyagari & Dr. Madhusudhana Subramanyam. This is a research/review paper, distributed under the terms of the Creative Commons Attribution-Noncom-mercial 4.0 Unported License http://creativecommons.org/licenses/by-nc/4.0/), permitting all noncommercial use, distribution, and reproduction in any medium, provided the original work is properly cited.

Omicronvirus Data Analytics using Deep Learning Technique

Mr. Anand Kumar Gupta[α], Dr. Asadi Srinivasulu[σ], Dr. Kamal Kant Hiran[ρ], Dr. Tarkeswar Barua[Ↄ], Mr. Goddindla Sreenivasulu[¥], Dr. Sivaram Rajeyyagari[§] & Dr. Madhusudhana Subramanyam[x]

ABSTRACT

The Man-made brainpower (AI) methods overall and convolutional brain organizations (CNNs) specifically have achieved victories in clinical picture examination and grouping. A profound CNN design partakes projected into this research article for the analysis of OMICRON grounded onto clinical radiography analysis (X-ray). As matter of fact the non-availability in adequate scope and excellent X-ray picture database, a compelling & exact Convolutional NN (CNN) characterization remained an examination. Managing those intricacies, for example, accessibility with a very-little measured and contrast database of picture resolution challenges, the database has pre-processed been into various stages utilizing various strategies to accomplish a powerful preparation database of the applied Convolutional NN (CNN) prototypical to achieve its finest presentation. Pre-processing phases in the database acted into research incorporate database adjusting, clinical specialists' picture investigation, and information expansion. The exploratory outcomes reveal general precision up to 98.08% that exhibits its great capacity of the prototypical Convolutional NN (CNN) system of the ongoing application space. Convolutional NN (CNN) prototype has tried been into 2 (two) situations. The primary situation explains that it has tried been utilizing the 7762 X-ray pictures as database, it accomplished a precision of 98.08 percent. To the subsequent situation, the prototypical has tried been utilizing the autonomous database of Omicron X-ray pictures from Kaggle. The execution into current assessment the situation remained just about 98.08%. It additionally demonstrates that the prototypical system beats different systems, as a similar examination has finished been thru a portion of AI calculations. The proposed model has superseded every one of the models by and large and explicitly when the model testing was finished utilizing a free testing set.

Keywords: omicron disease, cross-validation methods, classification algorithms, disease prediction, cnn, data minelaying, feature selection, data pre-processing.

Author α σ ρ Ↄ ¥ §: Azteca University, Data Science Research Laboratory, BlueCrest University College, Monrovia, Liberia.

I. BRIEF INTRODUCTION

The infection known as the extreme intense breathing disorder COVID-19 had found been in the year late 2020. The infection started in World turned into reason for an illness called as COVID-19 (Corona Virus Disease 2019). The pioneer organisation in health sector, WHO (World Health Organization), proclaimed of sickness as an epidemic declared in the month of March of the year 2020. As per intelligence records gave & refreshed by worldwide medical care specialists and state legislatures, the pandemic impacted large number of individuals globally most major disease brought about by COVID19 is connected with the lungs like pneumonia. The side effects via infection may fluctuate & incorporate respiratory disorders, high feverishness, fluid muzzle, and stroke. These clinical conditions may utmost generally been analyzed utilizing lung x-ray investigation of the irregularities. Radiography is an electromagnetic (x-radiation or x-beam or x-ray) type of infiltrating contamination that uses radio-emissions are gone over the ideal hominoid body

© 2022 London Journals Press

elements to make pictures of interior subtleties. The x-beam (x-ray) pictures are the portrayal of human's body interior organs/parts in highly contrasting shadows. The x-beams (x-rays) are the utmost established & ordinarily utilized clinical determination experiments. Lungs' x-beam is utilized into analyzing the chest and related illnesses such as lung sicknesses, breathing issues, pneumonia [4], etc. which gives a picture of thoracic hole, comprising of spine bones and chest alongside of delicate internal sensitive body parts together with the veins, airways, and lungs x-beam (x-ray) pictures strategy gives various advantages as a selective analysis technique of COVID19 compared with substitute examining procedures. Its advantages incorporate minimal expense, tremendous accessibility of x-beam (x-ray) facilities, harmlessness, less time utilization, and gadget moderateness. Thus, X-beaming can be well-thought-out a superior contender of mass, simple, & speedy analysis methodology to a global epidemic (also pandemic) such as COVID19 thinking about of ongoing worldwide medical services emergency. Profound learning and ANNs have supported a dramatic exploration center during the period of ten years and more. Profound Artificial NNs (ANNs) has superseded supplementary regular prototypes on numerous fundamental standards. Thus, Artificial NNs (ANNs) has commonly ended up being the cutting-edge innovation across a wide scope of use regions, including NLP, discourse acknowledgment, natural sciences, picture handling, other businesses, and scholarly extents headway for the Artificial NNs (ANNs) have gigantic possible into medical care applications, explicitly into clinical information examination, determination through clinical picture handling, and investigation. As found as of late, different regions of the planet face the medical care emergency both with regards to the required number of medical services experts and testing gear. Considering what is going on, there is a connection among recognizing COVID19 victims, lung x-beam picture investigation & characterization. In existing projected research, a programmed indicative framework has been created utilizing Convolutional NN (CNN) it utilizes lung x-beam examination outcomes to analyze if an individual is COVID19 impacted or ordinary. Fundamental investigation of the existing review have exposed satisfactory outcomes as far as its precision and other execution boundaries to analyze the sickness in a savvy and time-productive manner is review utilized Convolutional NN (CNN) thru additional flakes to further develops COVID19 x-beam picture characterization exactness. In brain organizations, the CNN structure is extraordinarily intended to handle the two-layered picture assignments in spite of the fact that it could likewise been utilized in 1-3 layered information. Preparing the CNN prototype, primarily, database has gotten been from GitHub.com.

II. LITERATURE SURVEY

Profound knowledge has exposed a sensational expansion into clinical utilizations overall & explicitly into clinical x-ray image-based conclusion. Profound training prototypes achieved unmistakably. Because of its exceptionally encouraging outcomes given by CNNs in clinical picture examination and grouping, they are considered as accepted norm in this area [9, 10]. CNN has been utilized for an assortment of order assignments connected with clinical analysis, for example, lung infection [10], discovery of disease (malarial) organism into pictures of tinny plasma cell [11], mammary gland cancer recognition [12], remote scanned pictures [13], mediate chest illness [14], determination of membrane malignant growth through characterization, & programmed finding the different lung sicknesses utilizing lung x-beam picture arrangement. Developments with COVID-19 in the Dec, 2019, various analysts were locked in the trial & error and exploration exercises connected with analysis, treatment, and the executives of COVID19. Scientists has detailed its meaning of relevance of Artificial Intelligence (AI) techniques into picture examination of the discovery and the board of COVID19 cases.

III. SYSTEM METHODOLOGY

3.1 Existing System

There are approachable in superficial learning strategies, for example, convolution neural

© 2022 London Journals Press

London Journal of Engineering Research

organization and intermittent neural organization. CNN computation Drawbacks: The disservices are:

1. Little precision
2. In flood Time Complexity
3. In flood Executing Time
4. In flood Error prone
5. Small Data Size

Computation downside

1. Little precision
2. In flood Time Complexity
3. In flood Execution Time
4. In flood Error prone
5. Little Data Size

3.2 Proposed System

There are available in deep learning method like Extended Convolutional Neural Networks i.e., in Deep Learning Technique.
ECNN algorithm Advantages:

1. In flood accuracy
2. Less time consuming
3. Little Performance Time
4. Little Mistake Degree
5. Big Data Scope

IV. INVESTIGATIONAL RESULTS

Basic idea is to execution, is to assure that the Omicron disease severer affected role collected statistics functioned in the way that can compel preparation, subdivision from their first outlook.

4.1 ECNN Algorithm

Two trials of one or the other CC or MLO seen should be adjusted utilizing the picture enlistment method. At that point, a distinction picture is got by deducting the earlier test from the current test and afterward scaled to the full-range force. The territorial pictures from the refined district proposition are trimmed from the three pictures and scaled to 224×224×3 for each picture, which are utilized for ECNN is floodlight extraction. The three channels are rehashed from one-channel grayscale pictures (e.g., current sweep of 224×224×1) since the pertained ECNN and ECNN models expect 3-channel pictures.

Multi-measurements of three-state in floodlights (from earlier sweep, current output, and contrast pictures) are made to prepare a CNN model. For instance, The ECNN is floodlights utilizing ResNet-60V3 of 2048×3 measurements for each view (CC or MLO) of a subject's side (left or right bosom). Remember that earlier sweep consistently relates to the ordinary (sound) status in any event, for a destructive subject. Assume we code sound and carcinogenic as 0 and 1 individually, at that point the ground realities (yields) compared to the three states (earlier, current, distinction) of a destructive view are [0 1 1]. This coding instrument can be handily stretched out to at least two earlier sweeps.

4.2 Algorithm

The following is the ECNN algorithm steps:
The Omicron disease infection data index, i.e., the absolute 522 pictures, our experiment involved the related following steps:

1. Introduces mandatory collection
2. Introduces training dataset
3. Executes in floodlight ordering of change data
4. Composition with 70-time phases and 2 yield
5. Introduce Keras deep learning library with all supporting bundles of the package
6. Resets ECNN
7. Enhances ERNN part & about regulation of loss calculation function.
8. Enhancement of yield part.
9. Adds the ECNN
10. Fits ECNN in the training dataset
11. Loads the Omicron disease infection test image data of the year 2020
12. Become a predicted Omicron disease infection in Dec 2019
13. Imagine aftereffects with anticipated or genuine Omicron disease infection

INPUT DATSET: Here the input dataset is having 14 columns with target class, i.e., severity level of the Omicron disease.

© 2022 London Journals Press

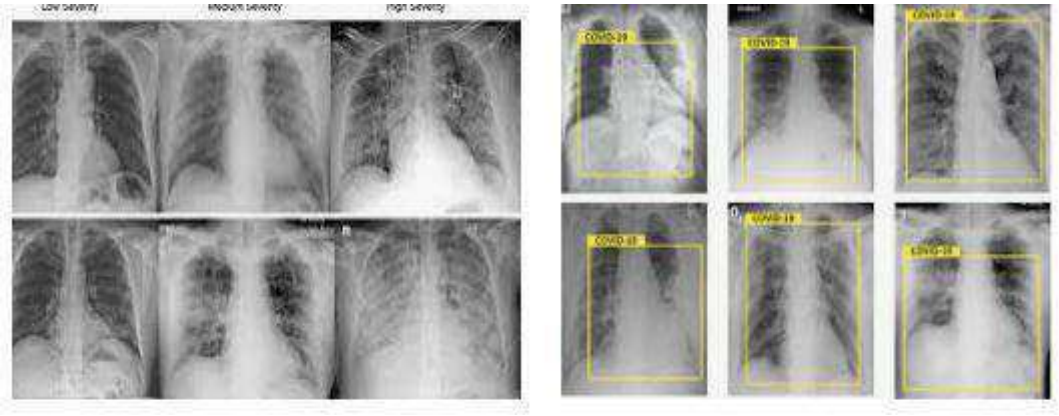

Figure 4.1: Input dataset, i.e., Omicron disease dataset of Proposed System

V. RESULTS

Here are the result of in finding Omicron disease detection by integrating ECNN.

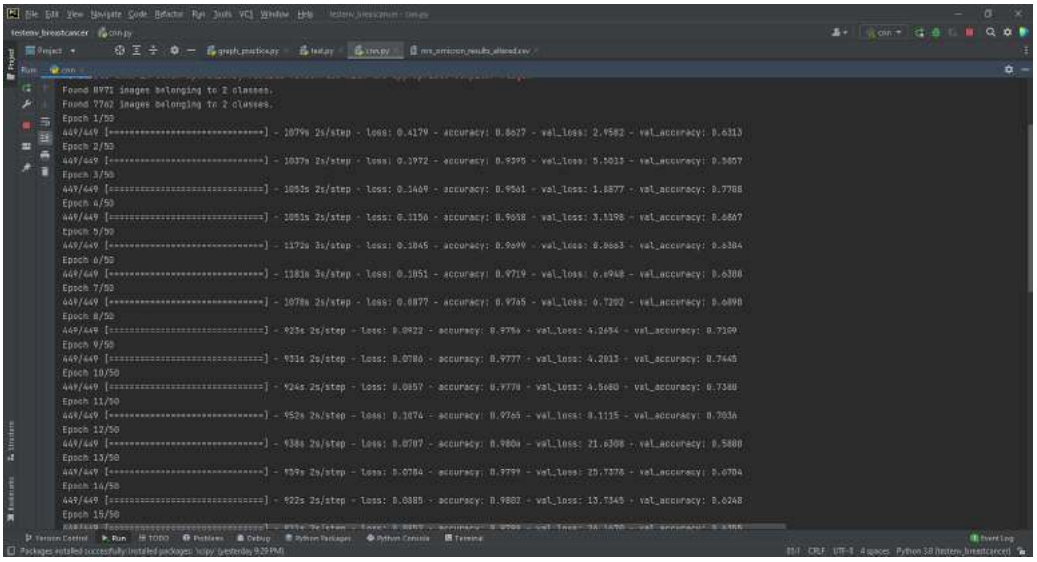

Fig. 4.1: Executing flow of ECNN

Fig 4.1 Exemplify the execution flow through Epoches on Omicron dataset

© 2022 London Journals Press

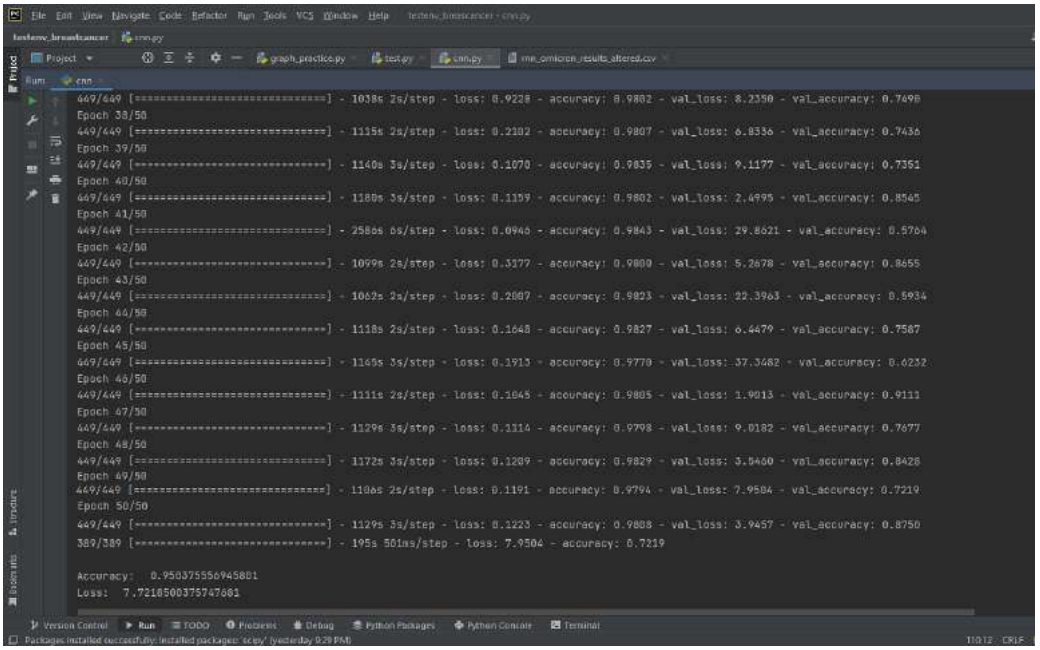

Fig. 4.2: Executing flow of Omicron disease sensing ECNN

Fig 4.2 Explains the final output on dataset from UCI, Google, Kaggle, Microsoft, Executing flow of through the epoches.

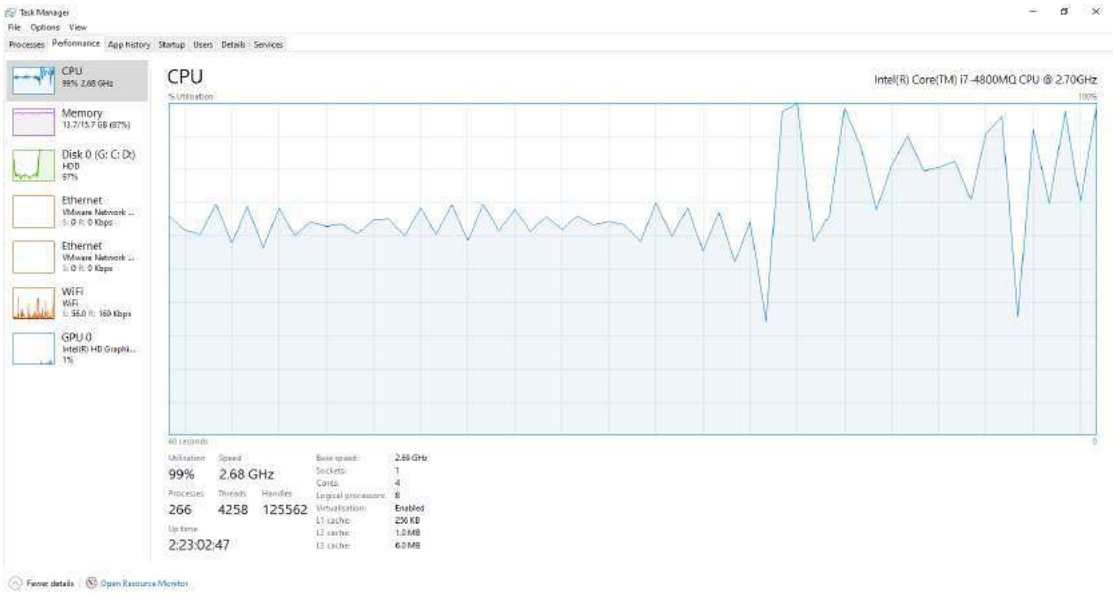

Fig. 4.3: CPU occupancy in the executing of ECNN with Windows OS

In the above figure it demonstrates the Processor occupancy rendering to the iterations with Epoches onto Omicron virus dataset with Windows OS.

© 2022 London Journals Press

Fig. 4.4: CPU occupancy for Omicron disease Dataset using ECNN with Linux OS

In the above figure it exemplifies processing power occupancy rendering to the amount of Epoches on Omicron illness with Linux OS.

5.1 Evaluation Methods

The following are measurements of evaluation methods or metrics.

$$Quality = \frac{BP+VM}{BP+VP+BM+VM}$$

$$Preciseness = \frac{BP}{BP+VP}$$

$$Callback = \frac{BP}{BP+VM}$$

$$F - measure = \frac{2xPrecisenessxCallback}{Preciseness+Callback}$$

Data Input: As previously said, our experiment will consider 6098 images.

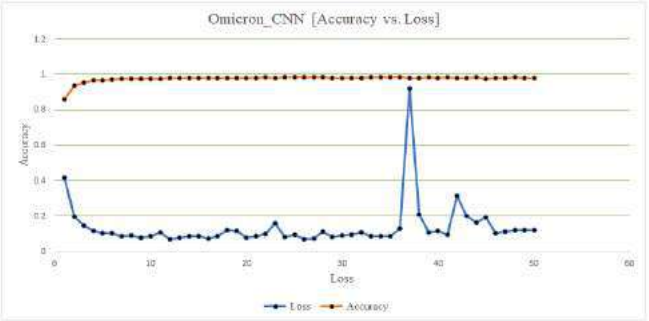

Figure 4.6: Omicron disease data Accuracy vs. Loss

Fig 4.6 Exemplify the executing epoches between Accuracy and Loss.

© 2022 London Journals Press

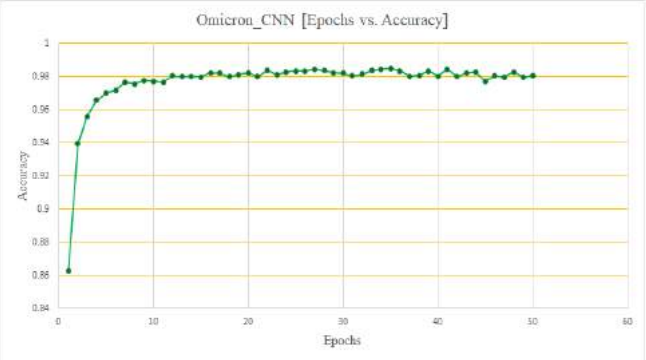

Fig. 4.7: Accuracy vs. Number of Epochs

Fig 4.7 lucubrate the executing epoches between Accuracy and number of iterations.

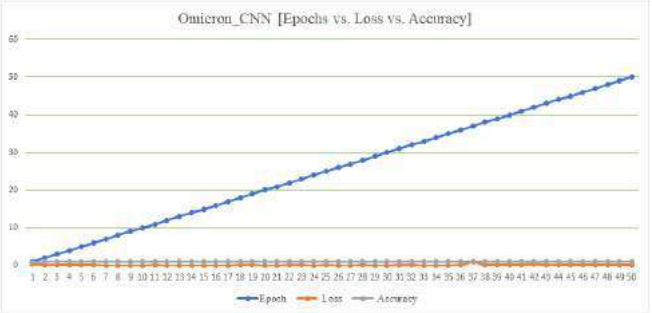

Fig. 4.8: Omicron Disease Dataset with Accuracy vs. Loss vs. Epoch

Fig 4.8 demonstrates the executing time between loss, Epochs and accuracy of the ECNN model.

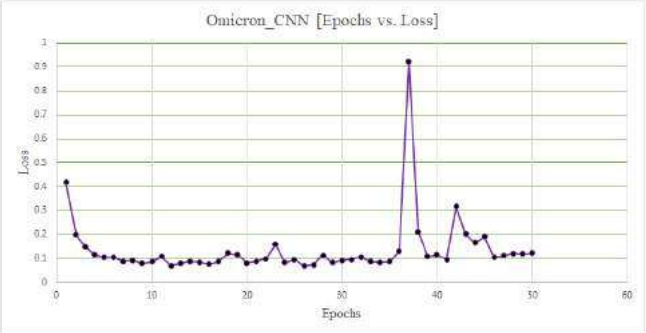

Fig. 4.9: Omicron disease dataset with Epochs vs. Loss vs. Epoch

Fig 4.9 Demonstrates the executing time between Epochs, loss and accuracy of the ECNN model.

© 2022 London Journals Press

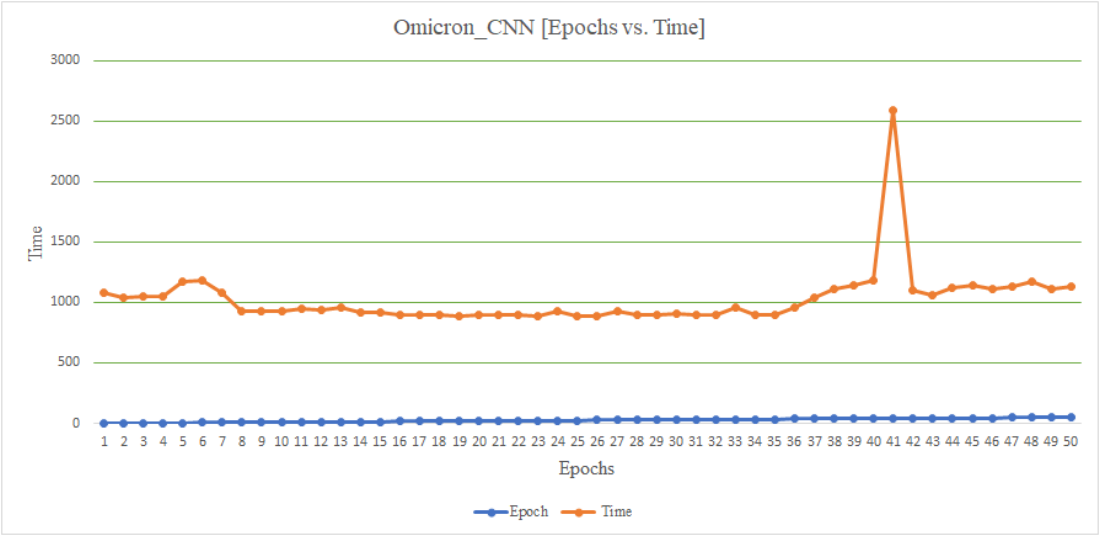

Fig. 4.10: Omicron Disease Dataset with Time vs. Loss

Fig 4.10 Demonstrates the executing time between Time and Loss of the ECNN model.

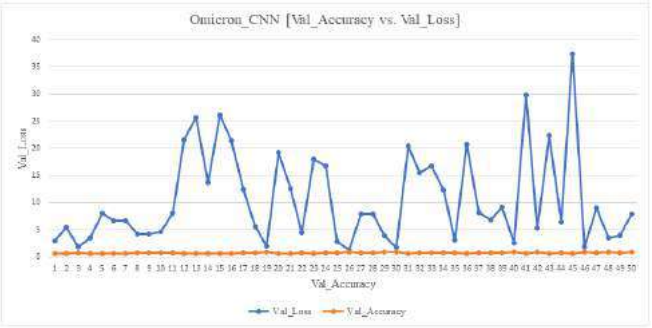

Fig 4.11: Omicron Disease Dataset with Time vs. Loss

Fig 4.11 Demonstrates the executing time between loss and Loss of the ECNN model.

V. CONCLUSIONS

This study has been directed to exhibit the powerful and precise analysis of Omicron utilizing ECNN which was prepared on chest X-beam picture dataset model preparation was performed gradually with various datasets to accomplish the greatest exactness and execution. Essential dataset was extremely restricted in size and furthermore imbalanced as far as class dispersion set problems thru the essential database impacted exhibition with model overview gravely. Towards conquering those problems, database had pre-processed utilizing various strategies, with database adjusting method, physical investigation thru x-beam pictures via appropriate clinical specialists & information expansion procedures. To adjust the database of prototype preparation then furthermore assessment of its presentation boundaries, a more than adequate amount of x-rays (chest) was gathered through various accessible causes. In the wake of preparing & testing the ECNN prototype upon the completely handled database, exhibition output has accounted been for. Likewise, for testing additional prototype execution, especially its exactness, the projected ECNN prototype have tried been utilizing autonomous database as a free approval & genuine examination acquired from organizations (such as IEEE) Data Portal. It is detailed into the outcomes of together the examination situations, the projected ECNN prototype have exposed profoundly encouraging outcomes. Hence this review involves a steady methodology in preparing the model utilizing various scopes & kinds of database, methodology

© 2022 London Journals Press

affirmed its way that ECNN prototypes entail adequate measure thru picture information for the productive and more-precise order. Information expansion procedures are extremely powerful to altogether further develop the ECNN model execution by creating additional information from a current restricted amount of database & furthermore via providing the capacity of differences with ECNN. Projected ECNN prototype's iterations of CNN layers were likewise settled into a gradual methodology; i.e., into the main addition, solitary CNN layer remained utilized, after that, at that point, based on model execution measurements, one layer in every augmentation was expanded till it arrives at a steady and productive stage regarding its presentation. A last adaptation of the ECNN comprised with 6 combined layers. Similar investigation have likewise been conducted additional examination to the extent with the projected ECNN prototype via execution examinations of a portion thru conspicuous AI systems like GBM, RF, SVC, KNN, and LR. The outcomes demonstrate projected ECNN have bypass everything the prototypes especially at times all prototypes were tried onto autonomous approved database. Bearing in mind that the huge impact by information expansion methods with prototype (model) exhibitions, creators is presently chipping away at the use of other best in class information increase calculations and procedures. Later on, the outcomes got from the review worried about the appropriateness of these cutting-edge information expansion strategies in various application spaces will be distributed.

REFERENCES

1. Aijaz Ahmad Reshi et al., "An Efficient CNN Model for COVID-19 Disease Detection Based on X-Ray Image Classification", Hindawi Complexity Volume 2021, Article ID 6621607, 12 pages https://doi.org/10.1155/ 2021/6621607.
2. D. Cucinotta and M. Vanelli, "WHO declares COVID-19 a pandemic," Acta Biomedica: Atenei Parmensis, vol. 91, pp. 157–160, 2020.
3. F. Rustam, A.A. Reshi, A. Mehmoodetal., "COVID-19future forecasting using supervised machine learning models," IEEE Access, 2020.
4. D. J. Cennimo, "Coronavirus disease 2019 (COVID-19) clinical presentation," vol. 8, pp. 101489–101499, 2020, https:// emedicine. medscape.com/article/2500114-clinical#b2, online. 2020.
5. X-ray (Radiography)-Chest, 2020, https:// www.radiologyinfo.org/en/info.cfm? Pgchestra#overview.
6. J. P. Cohen, "Github Covid19 X-ray dataset," 2020, https://github.com/ieee8023/covid-chestxray-dataset, 2020. Online.
7. Z. H. Chen, "Mask-RCNN detection of COVID-19 pneumonia symptoms by employing stacked autoencoders in deep unsupervised learning on low-dosehigh resolutionCT," IEEE Dataport, 2020.
8. A. S. Lundervold and A. Lundervold, "An overview of deep learning in medical imaging focusing on MRI," Zeitschrift f¨ur Medizinische Physik, vol. 29, no. 2, pp. 102–127, 2019.
9. M. Ahmad, "Ground truth labeling and samples selection for hyperspectral image classification," Optik, vol. 230, Article ID 166267, 2021.
10. B. Kayalibay, G. Jensen, and P. van der Smagt, "CNN-based segmentation of medical imaging data," 2017, http://arxiv. org/abs/1701.03056.
11. Q. Li, W. Cai, X. Wang, Y. Zhou, D. D. Feng, and M. Chen, "Medical image classification with convolutional neural network," in Proceedings of the 2014 13th International Conference on Control Automation Robotics & Vision (ICARCV), pp. 844–848, Singapore, December 2014.Dr. Asadi Srinivasulu, and Tarkeswar Barua "COVID-19 Virus Prediction Using CNN and Logistic Regression Classification Strategies", Journal of Data Analysis and Information Processing, 2022, 10, 78-89, ISSN Online: 2327-7203, ISSN Print: 2327-7211, DOI: 10.4236/ jdaip.2022.101005 Feb. 28, 2022, https://www.scirp.org/journal/jdaip/ (Scopus Journal).
12. Dr. Asadi Srinivasulu, and T. Sree Lakshmi," Malware Similarity Unveiling Using Twin Neural Networks", Design Engineering journal, ISSN:0011-9342, issue:01, Vol:01, pages: 1904-1916, February, 2022. https://

© 2022 London Journals Press

Infectious diseases-and-treatment.imedpub.com (Scopus Journal).
13. Dr. Asadi Srinivasulu, and Dr. Tarkeswar Barua, “Early Prediction of Covid-19 Using Modified Recurrent Neural Networks”, Journal of Infectious Diseases and Treatment (IPJIDT-21-P-7633), ISSN 2472-1093, Vol.7 No.8:7633, 2021.https://infectious-diseases-and-treatment.imedpub.com (SCI Journal).
14. Dr. Asadi Srinivasulu., Soora, N.R., Mohammed, S.W. et al. , “Prediction and detection of breast cancer text data using integrated EANN and ECNN techniques”, Appl Nanoscience (2021, Received22 July 2021, Accepted18 August 2021, Published01 September 2021). https://doi.org/10.1007/s13204-021-02033-whttps://link.springer.com/article/10.1007/s13204-021-02033-w#citeas– Springer Nature Journal.(SCI)
15. Dr. Asadi Srinivasulu, and Mr.Tarkeshwar Barua, “Early Prediction of Covid-19 using Modified Convolutional Neural Networks”, International Journal of Advanced Computational Engineering and Networking, ISSN (p): 2320-2106, ISSN (e): 2321-2063 Volume-9, Issue-4, Apr.-2021, http://iraj.in, http://iraj.in/journal/IJACEN//paper_detail.php?paper_id=17921&nameEarly_Prediction_of_Covid-19_using_Modified_Convolutional_Neural_Networks.
16. Dr. Asadi Srinivasulu Asadi and P. Satya Narayana et al,” A new algorithm for detection of nodes failures and enhancement of network coverage and energy usage in wireless sensor networks”, wireless sensor networks, Materials Today: Proceedings, https://doi.org/10.1016/j.matpr.2021.05.355. 2214-7853/2021 Elsevier Ltd., 5th, June 2021. (Elsevier) https://www.sciencedirect.com/science/article/pii/S2214785321039547.
17. Dr. Asadi Srinivasulu, and Ch, G., S., T., R., R., Sri Sai Satyanarayana, D., (2022), "Association of vaccine medication for the efficacious COVID-19 treatment", World Journal of Engineering, Vol. 19 No. 1, pp. 98-108. https://www.emerald.com/insight/content/doi/10.1108/WJE-01-2021-0062/full/html , 10th May 2021 (Scopus).
18. Dr. Asadi Srinivasulu, A., Ramanjaneyulu, K., Neelaveni, R. et al., “Advanced Lung Cancer Prediction Based on Blockchain Material Using Extended CNN”, Applied Nanoscience, APNA-D-21-00538, Received: 26 March 2021 /Accepted: 24 May 2021 Applied Nanoscience, (), 1-13, 10.1007/s13204-021- 01897-2, 09-06 http://link.springer. com/ article/10.1007/s13204 -021-01897-2 (SCI - Journal) – Springer Nature Journal.
19. Dr. Asadi Srinivasulu1, Surya Prasada Rao Borraaa, Vishal Moyalb et all, “An Efficient Shape Adaptive Techniques for the Digital Image Denoising”, Turkish Journal of Computer and Mathematics Education (Scopus-Journal), Vol.12 No.9 (2021), 2709-2719. https://doi.org/10.17762/turcomat.v12i9. 4328. https://www.turcomat.org/index.php/ turkbilmat/article/view/4328/3693.
20. Dr. Asadi Srinivasulu, Dr. Umesh Neelakantan, Tarkeshwar Barua, “Early Prediction of Lung Cancer Detection Using Extended Convolutional Neural Networks”, ISSN: 00333077, Psychology and Education (2021) 58(1): 5614-5624, Article Received: 18 October 2021, revised: 6 February 2021, Accepted: 20 January 2021. https://doi.org/10.17762/pae.v58i1.1966, http://psychologyandeducation.net/pae/index.php/pae/article/view/1966. (Scopus – Journal).
21. Dr. Asadi Srinivasulu1 and Gangadhar Ch et al, “Association of vaccine Medication for the Efficacious COVID-19 Treatment”, World Journal of Engineering, Vol. ahead-of-print No. ahead-of-print. https://doi.org/10.1108/WJE-01-2021-0062 (Scopus – Journal).

© 2022 London Journals Press

Scan to know paper details and
author's profile

Modelling of the Resilient Modulus (Mr) of Lateritic Soils in Tropical Africa (Burkina Faso and Senegal): Determination of Model Parameters K1, K2 and K3 (Thom and Brown (1987), Uzan (1985) and the NCHRP 1-28A (2004) (National Cooperative Highway Research Program)

KI Bibalo Ida Josiane, BA Makhaly & COULIBALY Mory

University Ibar Der Thiam

ABSTRACT

The study of the cyclic behavior of materials has been very successful with the development of increasingly powerful computer tools that allow to limit costly experimental studies in favor of numerical models. This development has led to an increasing demand from the scientific community in terms of accuracy of numerical simulations and in terms of calculation time. The numerical tool allows to simulate the material behavior based on plastic, viscoplastic or elastoplastic behavior models [1]. Our study will focus on the determination of the parameters of three models used for the determination of the reversible moduli (Mr).

Keywords: lateritic soil; cyclic triaxial repeated loading (TCR); measured (Mrm) and predicted (Mrp) resilient modulus; k1, k2, k3 model parameters.

Classification: DDC Code: 631.4 LCC Code: S592.2

Language: English

London Journals Press

LJP Copyright ID: 392913
Print ISSN: 2631-8474
Online ISSN: 2631-8482

London Journal of Engineering Research

Volume 22 | Issue 5 | Compilation 1.0

© 2022. KI Bibalo Ida Josiane, BA Makhaly & COULIBALY Mory. This is a research/review paper, distributed under the terms of the Creative Commons Attribution-Noncom-mercial 4.0 Unported License http://creativecommons.org/licenses/by-nc/4.0/), permitting all non-commercial use, distribution, and reproduction in any medium, provided the original work is properly cited.

Modelling of the Resilient Modulus (Mr) of Lateritic Soils in Tropical Africa (Burkina Faso and Senegal): Determination of Model Parameters K1, K2 and K3 (Thom and Brown (1987), Uzan (1985) and the NCHRP 1-28A (2004) (National Cooperative Highway Research Program)

KI Bibalo Ida Josiane[α], BA Makhaly[σ] & COULIBALY Mory[ρ]

ABSTRACT

The study of the cyclic behavior of materials has been very successful with the development of increasingly powerful computer tools that allow to limit costly experimental studies in favor of numerical models. This development has led to an increasing demand from the scientific community in terms of accuracy of numerical simulations and in terms of calculation time. The numerical tool allows to simulate the material behavior based on plastic, viscoplastic or elastoplastic behavior models [1]. Our study will focus on the determination of the parameters of three models used for the determination of the reversible moduli (Mr). These models are those of Thom and Brown [2], Uzan [3] and the NCHRP [4] (National Cooperative Highway Research Program) of the MEPDG (Mechanistic-Empirical Pavement Design Guide) which are a function of the loading level (the confining stress (σ_3), the deviatoric stress (σ_d), the octahedral stress and the total stress (θ)). The research will be carried out on 4 samples of lateritic gravelly soils, 2 of which are from Burkina Faso (the Badnogo and Dédougou sites) and 2 from Senegal (the Sindia and Lam-lam sites). We carried out cyclic triaxial tests with repeated loading (TCR) according to the European standard Nf EN-13286-7 [5]. The tests were performed at variable confining stress to calculate the measured Reversible Modulus (Mrm = $\sigma_d / \varepsilon_{1,r}$).

The materials studied have a maximum diameter of 20 mm and a percentage of fines lower than 20%. The samples are compacted to three water contents (w_{opm} - 2%, wopm and w_{opm} + 2%) and to an optimum dry density (γ_{dopm}) equal to 95% and 100%. The methodology used was least squares ($\Sigma(\Delta Mr)^2$) and iteration by the "non-linear GRG" solving method used by the Solver calculation engine in Excel software. This allowed us to determine the values of the parameters k_1 (in kPa and > 0), k_2 (unitless and < 0), k_3 (unitless and > 0) of the above numerical models. It is found that the k_1, k_2, k_3 parameters and correlation coefficients are on average equal to 3511.540 kPa, -0.420, 0, and 0.91 for Thom and Brown's model [2]; 4988.974 kPa, -0.289, 0.536, and 0.97 for Uzan's model [3]; and 2436.959 kPa, -0.398, 1.864, and 0.91 > 0.90 for NCHRP [4] respectively. The predicted summary reversible modulus (MRSP) by the NCHRP model [4] is on average equal to 377.543 MPa. On the other hand, for the materials Ded/9.93/95.42 and Ded/8.16/95.39 the parameter k1 increases by 37.83% and the modulus MRSP also increases by 39.26%.

Moreover, for Ded/8,16/95,39 and Ded/6,23/95, 52 the k1 parameter increases by 65,77% and the MRSP module also increases by 39,11%. This justifies that the parameter k1 tells us about the hardening effect of the material.

Keywords: lateritic soil; cyclic triaxial repeated loading (TCR); measured (Mrm) and predicted (Mrp) resilient modulus; k_1, k_2, k_3 model parameters.

© 2022 London Journals Press

Author α σ: University Ibar Der Thiam "Laboratoire de Mécanique et Modélisation" (L2M) of Department of engineering Sciences, Cité Malick SY Route du CNEPS Villa N°100, Thiès BP 967, Senegal.

I. INTRODUCTION

The resilient behavior of granular materials is affected by several factors, the most important of which is the level of stress applied. It is so essential that the stress-deformation relationship be modelized exactly with mathematical laws to predict the long and short term behavior as well as the performance of granular materials. The simplicity of the material response analysis procedure makes it difficult to establish models that respect the theoretical principles of soil mechanics [6]. The resilient modulus (MR) of road materials is one of the most important parameters in the analysis and design of pavements.This parameter is used in empirical and mechanistic-empirical methods as the main parameter to express the stiffness and behavior of road construction materials. To determine this parameter in the laboratory, it is necessary to perform a dynamic triaxial loading test under different confinement and deflection constraints, which is a costly and time-consuming approach [7]. To overcome these very exorbitant costs, several researchers have developed digital models such as Thom and Brown [2], Uzan [3] and the NCHRP (National Cooperative Highway Research Program) [4] that we studied in our research.

However, the objective of this work is to determine their parameters. For this we based ourselves on the experimental results to calculate the measured resilient modulus (Mrm), in order to predict the resilient modulus (Mrp) by the aforementioned digital models and determined their parameters. One of the most important aspects for the design and sizing of pavements is the elastic or resilient modulus (MR) which allows to characterize the mechanical behavior of materials necessary for the sizing of a pavement (AASHTO American Association of State Highway and Transportation Officiais 1986 [8]). Studies on gravelly lateritic rocks have rarely been reported in the literature. The only works to be found are those of ((Sikali et al. (1980) and Sweere et al. (1990) in [9]). To this can be added the work carried out in Senegal during the last two years. decades to discover the advanced parameters of granular materials (Fall, Ba, Samb, Dione, and Aïdara [10]) have contributed to deepening knowledge on the advanced mechanical behavior of road materials used in Senegal. In order to contribute to the improvement of the technical documents used for the design and dimensioning of pavements in tropical Africa, we carried out cyclic triaxial repeated loading tests (TCR) of the SCHENCK brand at the Gustave Eiffel University in Nantes in s " based on European standard EN 13286-7 [5] while maintaining the variable confinement pressure (method A). The measured stress-strain results are interpreted for the resilient part by applying the Boyce model, extended to the axial anisotropy [10]. The materials used come from Burkina Faso and Senegal and are of a gravelly lateritic nature, class B4-B6 according to the GTR classification.

II. MATERIALS AND METHOD

About two hundred years ago the term "laterite" first appeared in the scientific literature. Despite various vicissitudes, this term is still widely used. We could think that it covers perfectly recognized and defined facts. However, a study, even a brief one, of synthetic works dealing with this problem shows that, under the brevity of the term, sometimes very different objects are hidden. It is therefore useful to first look at the definitions that have been given to this term. We will then discuss the soil formation processes called "laterites" and their location in the world [11]. In local dialects these formations are called "brick earth". The name "laterite" is therefore only the Latin translation of a vernacular terminology.

2.1 Classification of materials used

- *General information on lateritic soils*

Laterite has the root "later" which means brick in Latin, this only by reference to the use of these blocks (Maignien, 1966; Autret 1983; Bourgeon & Gunnell, 2005 in [12]).

Theories dealing with the origin and formation of laterites are varied. Nowadays, the definition which seems to be unanimous among authors is

© 2022 London Journals Press

that of Schellman in 1986 in [13] because it is based on the conditions of alteration of the bedrock and the mineralogical composition. For this author: "Laterites are products of intense meteoric weathering and are made up of a mineral assemblage that can be made of goethite, hematite, aluminum hydroxide, kaolinite and quartz" figure 1 ". The SiO2 / (Al2O3 + Fe2O3) ratio compared to that of the parent rock must be such that the laterite formation does not contain more silica than that which is retained in the remaining quartz and that which is necessary for the formation of kaolinite "[13].

Laterites are widely distributed throughout the world, but more particularly in intertropical regions of Africa, Australia, India, Southeast Asia and South America. Laterites extend beyond subhumid tropical climates and can be observed even in desert regions (African and Australian deserts) where they point to wetter past influences. Considering that the intertropical zone covers 40% of the terrestrial surface of the globe, the lateritic cover is estimated at 33% of the surfaces of the continents, in addition to the desert zones and the steppe zones where laterite does not form (Tardy, 1997 in [14] “figure 2”.

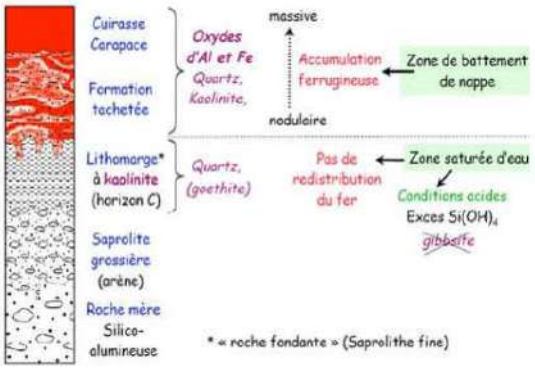

Fig. 1: Lateritic profile (Retallack, 1997 in [14])

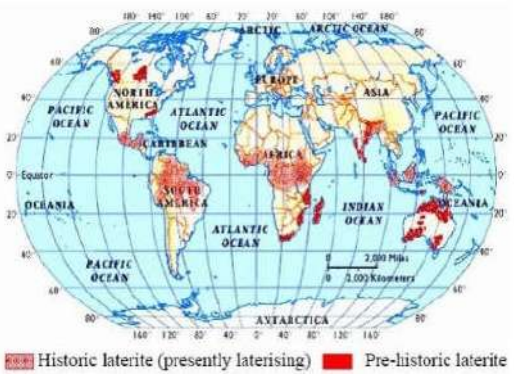

Fig. 2: current and prehistoric laterites (Persons, 1970 in [12])

- *Characterization of laterites from Senegal and Burkina Faso used*

The study as a whole focused on the laterites of two borrowings sites in Burkina Faso (Badnogo and Dédougou) “figure 3” and of two (2) quarries in Senegal (Sindia and Lam-Lam) “figure 4”. The laterites and many other soils of the intertropical regions are located in areas where it is very hot and where the rains are abundant, either all year round or during a wet season (Legros, 2013 in [15]).

The summary of the material characterization tests is presented in "Table 1". It appears that:

After analysis of the materials, it can be seen that the samples, despite the diversity of their origin, are gravelly materials with little clay (lateritic gravels with little clay) and of class B4, B5 and B6 "table 1" according to the book of the "Guide of Road Earthworks "[10].

Fig. 3: location of borrowing sites in Burkina Faso (Dédougou et Badnogo)

© 2022 London Journals Press

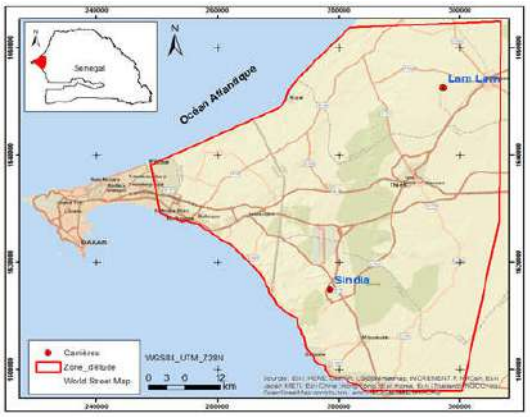

Fig. 4: location of borrowing sites in Senegal (Sindia et Lam-Lam

Table 1: Physical and mechanical characterization of lateritic soils samples [10]

Designation of borrow sites	Particle size Analysis				Materials classification				Parameters of the Atterberg limit			CBR compactness and lift parameters				
	Sand (%)	Fines (%)	Ratio									Water content	Dry density	Parameters of the Modified Proctor		CBR after 4 days of immersion
	2 mm	80 µm	Cu	Cc	GTR	LCPC	AASHTO	USCS	LL (%)	PI (%)	Ic	wn (%)	Gs	γd max (kN/m3)	wopm (%)	95% OPM
Sindia	41.6	17.86	207	0.34	B5	GA	A2-4a (0)	GC - CL	29.85	9.2	2.7	4.7	2.76	19.7	9.66	54.8
Lam-Lam	39.3	18.19	130	0.28	B5	GA	A2-4a (0)	GC - CL	30.3	10.1	2.4	5.6	2.69	17.52	11.8	30.5
Dedougou	25.2	10.21	763	29.5	B4	GA	A2-4a (0)	GM - GC	27.5	7.2	3.2	4.3	2.82	22.5	8.05	65
Badnogo	34.6	16.63	129	11.6	B6	GA	A2-6 (0)	GC - CL	28	13	1.8	4.6	2.76	21.45	9.7	58

2.2 Methodology of the cyclic triaxial test with repeated loading

Like Untreated Graves, laterites are natural granular materials without binder, which exhibit a highly non-linear behavior, depending on the stresses applied and the number of loading cycles. The triaxial repeated loading test is widely used to study the mechanical behavior of these types of materials [16]. The TCR consists in subjecting a cylindrical specimen of untreated granular material to cyclic loadings, simulating the stresses existing in a road bedding layer, and in measuring the axial and radial deformations of the specimen produced by these phase loads. The standard used is EN 13286-7 [5] and defines three different test procedures (method B with constant confining pressure σ3, method A with variable confining pressure σ3 and stepwise method the one we have used). From the identification and characterization tests (particle size, Atterberg limit, Proctor, etc.) we notice that the laterites are close to the GNT. This justifies the choice of this aforementioned standard [10].

For entering the input data for the confinement stress, we deduce 2kPa. This corresponds to the weight of half the height of the water contained in the cell. The test pieces after preparation to the desired water content and density of compactness are assigned the sensors for measuring axial and radial deformations “figure 5” and “figure 6”.

© 2022 London Journals Press

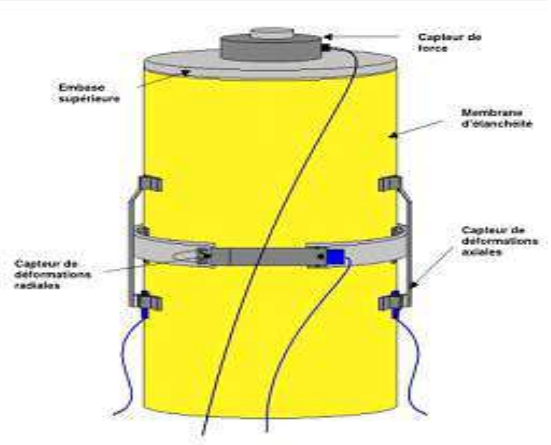

Fig. 5: Complete device for measuring axial and radial deformations [16]

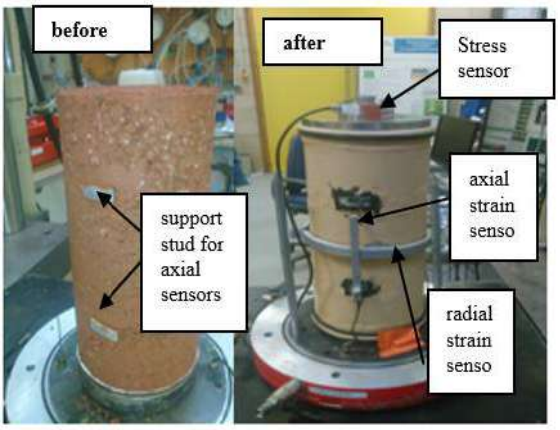

Fig. 6: Test specimen with sensor fixing studs (before) and with sensor installation (after)

III. MODELING BY SEVERAL NO LINEAR MODELS OF THE RESILIENT MODULUS

The resilient behavior of granular materials is affected by several factors, the most important of which is the level of stress applied; where they exhibit no linear behavior. It is essential that the stress-strain relationship be modelized exactly with mathematical laws to predict the long and short term behavior as well as the performance of granular materials. The simplicity of the material response analysis procedure makes it difficult to establish models respecting the theoretical principles of soil mechanics (Lekarp et al., 2000 in [17]).

To take into account the non-linearity of bass behavior, the modulus of elasticity is replaced by the Resilient Modulus (Seed et al., 1965 in [17].). The term "resilient" refers to the portion of the recoverable energy of a material that is stressed, when it is discharged. This is how the resilient modulus concept was developed to allow better simulation of the loading of pavements by rolling loads [14].

Lekarp, Isacsson, & Dawson [6] reported on numerous studies carried out since 1960 in order to characterize the resilient behavior of granular materials. The studies found in the literature, show that this behavior can be affected, with different degrees of importance, by several factors such as the level of stress, the history and number of loading cycles, the loading frequency, the effect of density, grain fraction and grain shape, water content. However, the most important parameter affecting the resilient response is the level of stress applied to the sample (Table 2.1) [14].

3.1 No linears models of resilient modulus used

An elastic constitutive law is chosen, can be elastic linear isotropic (from the normative point of

© 2022 London Journals Press

view), hypo elastic (model K-θ) or hyper elastic (model of Boyce) [18]. There are several digital models used in the bibliography for the digital modeling of the resilient module. These models are either according to the level of loading or according to the physical parameters. The methodology used is that of least squares (Σ (ΔMr) ²) and iteration by the "no linear GRG" resolution method used by the Solver calculation engine in the Excel software. This allowed us to determine the values of the parameters k_1 (in kPa and> 0), k_2 (without unit and <0), k_3 (without unit and> 0) of the aforementioned numerical models.

We determine the residual (Ri) by equation 1 which will be the objective to be defined in the Solver and the variable cells which correspond to the cells of the parameters k_i to be determined.

$$Ri = \frac{\left(\sum_{i=1}^{n}(\Delta Mr)_i^2\right)}{Nb} = \frac{\left(\sum_{i=1}^{n}(Mr_m - Mr_p)^2\right)}{Nb} \quad (1)$$

Ri is the residual, Mrm the measured modulus, Mrp the modulus predicted by the chosen model and Nb corresponding to the matrix of cells (number of sequences).

Several models have been developed for the prediction of the resilient modulus of untreated bass (GNT). Among which we have:
Uzan [3] proposes a modification of the k - θ model to take into account the effect of the deviatoric stress. This relationship is expressed by equation (2) as follows:

$$M_r = k_1 p_a \left(\frac{\theta}{p_a}\right)^{k_2} \left(\frac{\sigma_d}{p_a}\right)^{k_3} \quad (2)$$

k_1, k_2 et k_3 are parameters of model pa is atmospheric pressure in kPa;
θ = sum of principal stresses in k Pa is the deviatoric stress in kPa

Uzan's model seems to agree well with the experimental results on GNT even at confinement stresses greater than the deviatoric stress
Thom and Brown [2] experiment the Resilient Modulus as a function of the following stress ratio according to the equation:

$$M_r = k_1 \left(\frac{p}{q}\right)^{k_2} \quad (3)$$

k_1, k_2, are the parameters of the model, $q = \sigma_d = \sigma_1 - \sigma_3$ deviatoric stress, p = average pressure ($p = (\sigma1+\sigma2+\sigma3) / 3$).

A new "harmonized" test protocol for the resilience module has been developed as part of the NCHRP project 1-28A [4]. This model, called either the NCHRP model or the MEPDG model, is implemented in the new "Mechanistic-Empirical Pavement Design Guide" (MEPDG). This new protocol uses the universal nonlinear model which is applicable to unbound base or subbase materials given by equation (4) [17]. This equation combines the hardening effect of the sum of the principal stresses and the softening effect of the shear stress; thus, the value of k2 must be positive and that of k3 negative. But in our study for severe lateritics the value of k2 will be negative and that of k3 positive. To properly identify the model constants, the multiple correlation

© 2022 London Journals Press

coefficients determined for the test must exceed 0.90. It should be noted that the use of this model is proposed for both the granular materials of the base layers and for the fine soils of the foundation layers.

$$M_r = k_1 pa\left(\frac{\theta}{pa}\right)^{k_2} \cdot \left(\frac{\tau_{oct}}{pa}\right)^{k_3} \quad (4)$$

k_1, k_2, k_3 are the parameters of the model. ($k_1 > 0$; $k_2 < 0$; $k_3 > 0$ for our lateritic materials.

3.2 The results obtained and interpretations

It appears that:

- After the analysis of the materials, it can be seen that the samples, despite the diversity of their origin, are gravelly materials with little clay (lateritic gravels with little clay) and of class B4, B5 and B6 according to the book of the "Guide de Terrassement Routier "Table 1»
- Table 2 and figures 7 (a), 7 (b) and 7 (c) show that the parameter k1 is positive and varies according to the type of material and the type of model. Their maximum, average and minimum values are represented by diagrams in « Box »
- Table 2 and figures 8 (a), 8 (b) and 8 (c) show that the parameter k2 is negative and varies depending on the type of material and the type of model. Their maximum, average and minimum values are represented by diagrams in « Box »
- Table 2 and figures 9 (a), 9 (b) and 9 (c) show that the correlation coefficient R varies according to the type of material and the type of model. Their maximum, average and minimum values are represented by diagrams in « Box ». We deduce that:
- Figure 10 shows a regression curve of the measured Resilient Modulus (Mrm) against the predicted Resilient Modulus (Mrp) of the models: (Uzan [3], Thom and Brown [2], NCHRP [4]) of the sample Sin 12.10 / 95.75. We deduce that the Uzan model is closer to the line of equation Y X, from which it correlates well especially for the material Sin / 11.7 / 95.71 with a correlation coefficient equal to 0.994.
- The parameters k_1, k_2, k_3 are on average respectively equal to 3511.540 kPa, -0.420, 0, and 0.91 for the model of Thom and Brown [2]; 4988.974 kPa, -0.289, 0.536 and 0.97 for that of Uzan [3] and 2436.959 kPa, -0.398, 1.864 and 0.91 for the NCHRP [4] « Table 2 ».
- The summary resilient modulus predicted by the NCHRP model [4] is on average equal to 377.543 MPa for the four samples « table 2 ».
- In addition, table 2 shows us that for the materials Ded / 9.93 / 95.42 and Ded / 8.16 / 95.39 the parameter k1 increases by 37.83% and the MRSP modulus also increases by 39.26 %. In addition, for Ded / 8.16 / 95.39 and Ded / 6.23 / 95.52, the parameter k_1 increases by 65.77% and the MRSP modulus also increases by 39.11%. This justifies that the parameter k_1 tells us about the hardening effect of the material.

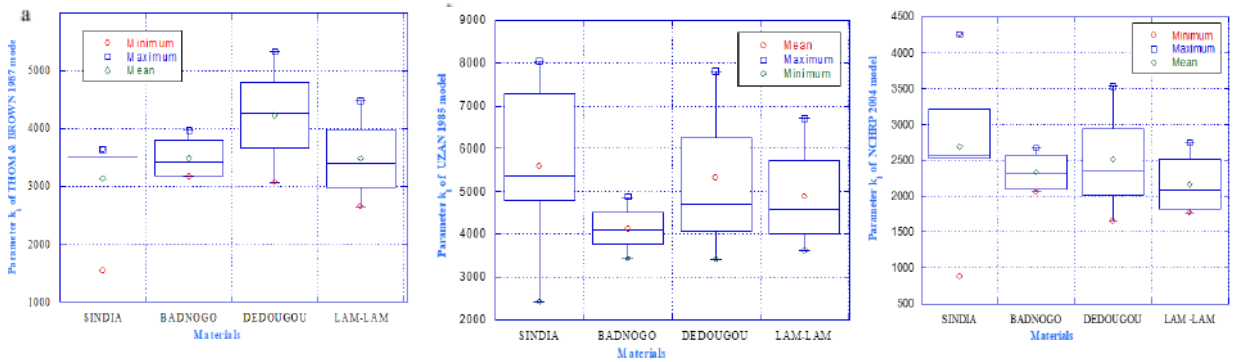

Fig. 7: Parameter k_1 (a) of the Thom and Brown model [2]; (b) of the Uzan model [3]; (c) of the NCHRP model [4]

© 2022 London Journals Press

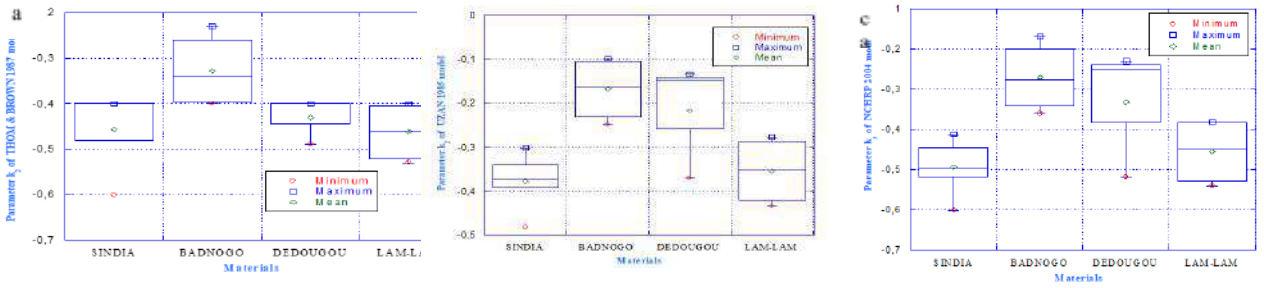

Fig. 8: Parameter k_2 (a) of the Thom and Brown model [2]; (b) of the Uzan model [3]; (c) of the NCHRP model [4]

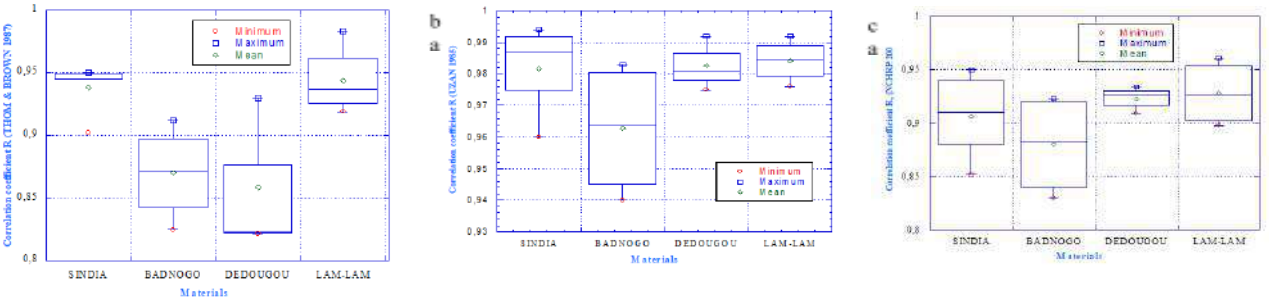

Fig. 9: correlation coefficient (a) of the Thom an Brown model [2]; (b) of the Uzan model [3]; (c) of the NCHRP model [4]

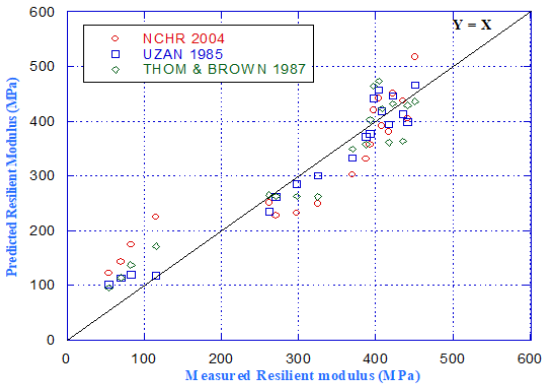

Fig. 10: Resilient Modulus measured / Resilient Modulus predicted by the models (UZAN [3], THOM and BROWN [2], NCHRP [4]) of the Sin sample 12.10 / 95.75

© 2022 London Journals Press

Table 2: Summary of the parameters and correlation coefficient and determination of the digital models of the resilient module

Name		Model of THOM & BROWN 1987		Coefficients		Model of UZAN (1985)			Coefficients		Model of NCHRP (2004)			Coefficients		Predicted Resilient Modulus Sommary (MRSP) (MPa) $\theta = \sigma_b$ 208 kPa τ_{oct} = 48,6 kPa $\sigma_3 = \sigma_c$ = 35 kPa
		k_1	k_2	Correlation	Determination	k_1	k_2	k_3	Correlation	Determination	k_1	k_2	k_3	Correlation	Determination	
SINDIA Wop%= 9,66	Sin/11,7/95,71	1532,67	-0,60	0,902	0,814	2421,05	-0,482	0,860	0,994	0,988	874,634	-0,601	2,606	0,95	0,905	158,496
	Sin/12,10/95,75	3489,45	-0,40	0,945	0,894	4798,57	-0,301	0,454	0,975	0,950	2567,506	-0,412	1,632	0,91	0,822	363,430
	Sin/9,90/95,80	3635,15	-0,48	0,949	0,900	5356,91	-0,371	0,568	0,987	0,973	2525,042	-0,496	1,957	0,852	0,923	382,110
	Sin/9,10/94,94	3489,45	-0,396	0,945	0,894	8032,71	-0,340	0,465	0,960	0,922	4253,516	-0,446	1,644	0,880	0,775	590,010
	Sin/7,59/95,94	3489,45	-0,40	0,945	0,892	7279,08	-0,391	0,642	0,992	0,984	3210,334	-0,516	2,124	0,940	0,884	511,592
BADNOGO 2 Wop% = 9,7	Bad/11,43/95,48	3608,36	-0,23	0,864	0,746	4083,44	-0,106	0,265	0,938	0,879	2669,361	-0,225	1,175	0,835	0,697	361,414
	Bad/10,04/95,58	3167,07	-0,29	0,825	0,680	3438,19	-0,099	0,372	0,945	0,893	2058,260	-0,174	1,295	0,855	0,730	303,366
	Bad/7,57/95,32	3973,45	-0,40	0,883	0,780	4872,05	-0,215	0,516	0,983	0,967	2476,969	-0,322	1,749	0,923	0,853	392,118
	Bad/9,36/100,06	3203,82	-0,39	0,912	0,833	4119,91	-0,249	0,484	0,978	0,956	2143,762	-0,360	1,698	0,917	0,840	323,581
DEDOUGOU Wop% = 8,05	Ded/9,93/95,42	3068,14	-0,40	0,822	0,676	3413,88	-0,148	0,568	0,992	0,984	1655,390	-0,249	1,847	0,934	0,873	287,385
	Ded/8,16/95,39	4269,22	-0,40	0,823	0,677	4704,63	-0,134	0,538	0,981	0,963	2358,181	-0,231	1,757	0,909	0,827	400,204
	Ded/6,23/95,52	5329,26	-0,49	0,930	0,865	7799,18	-0,370	0,601	0,975	0,950	3530,922	-0,518	2,101	0,926	0,858	556,713
LAM-LAM Wop%= 11,8	Lam/14,56/95,21	3489,45	-0,51	0,983	0,965	4762,95	-0,434	0,579	0,992	0,983	1765,563	-0,515	2,562	0,961	0,923	334,751
	Lam/12,43/98,92	3308,74	-0,40	0,932	0,869	4403,64	-0,277	0,485	0,983	0,966	2276,177	-0,385	1,699	0,907	0,823	337,386
	Lam/13,92/96,51	2647,89	-0,41	0,941	0,885	3629,59	-0,297	0,472	0,976	0,953	1882,254	-0,382	1,655	0,898	0,807	274,747
	Lam/10,15/96,04	4483,07	-0,53	0,919	0,844	6707,81	-0,408	0,709	0,986	0,972	2743,480	-0,542	2,320	0,946	0,895	463,386

© 2022 London Journals Press

IV. CONCLUSION

At the end of our research we can conclude that the gravelly lateritic materials, despite their geographic diversity, have almost the same physical and compact characteristics; they are class B4, B5 and B6 according to the GTR classification. In addition, after testing the cyclic triaxial (TCR) by standard EN 13286-7 [5] with method A, the resilient molds obtained differ from the type of materials (percentage of fine, water content, and stress level. Three mathematical models were used in our work for analysis. The Resilient modulus measured (Mrm) with respect to the Resilient modulus predicted (Mrp) by these models (Uzan [3], Thom and Brown [2], NCHRP [4]) tells us that the Uzan model [3] presents a very good correlation whatever the material, especially for the Sin / 11.7 / 95.71 material with a correlation coefficient equal to 0.994. In addition, the parameters k1, k2, k3 are at least respectively equal to 1532.670 kPa, -0.600, 0, and 0.82 for the model of Thom and Brown [2]; 2421.050 kPa, -0.482, 0.265 and 0.94 for that of Uzan [3] and 874.634 kPa, -0.601, 1.175 and 0.84 for the NCHRP [4]. The summary resilient modulus predicted by the NCHRP model [4] is on average equal to 377.543 MPa for the four samples. We also notice that for the materials Ded / 9.93 / 95.42 and Ded / 8.16 / 95.39 the parameter k1 increases by 37.83% and the MRSP modulus also increases by 39.26%. In addition for Ded / 8,16 / 95,39 and Ded / 6,23 / 95,52 the parameter k1 increases by 65.77% and the MRSP modulus also increases by 39.11%. This justifies that the parameter k1 tells us about the hardening effect of the material.

In perspective, propose to strengthen studies by determining the SiO_2 / (Al_2O_3 + Fe_2O_3) ratio and other chemical and mineralogical mechanical tests in order to better classify our material.

ACKNOWLEDGEMENTS

Firstly I say thank you to my creator God of the visible and invisible universe. Secondly, my gratitude goes to the staff of the Laboratory, Auscultation, Modeling, Experimentation, Transport Infrastructures (LAMES) of the campus of the Gustave Eiffel University of Nantes, formerly the IFSTTAR institute of Nantes, who accompanied me in the realization of triaxial tests (TCR). Furthermore, I would like to thank the staff of the Laboratoire National du Bâtiment et des Travaux Publics (LNBTP) of Burkina Faso as well as the staff of the Laboratoire de Mécanique et de Modélisation (L2M); of the doctoral school (ED2DS) of the University Iba Der Thiam of Thiès in Senegal (Unité de Formation en Sciences de l'Ingénieur). Thirdly, I reiterate my gratitude to the National Fund for Education and Research (FONER) of Burkina Faso for their financial support. Finally, I would like to reiterate my thanks to all the people who contributed to the realization of this work.

REFERENCES

1. Djimli, L., Analyse du phénomène de rochet : essais et modélisation. INSA de Rouen; Université Mentouri Constantine, Algérie 2020.
2. NH Thom, SF Brown Effect of moisture on the structural performance of a crushed-limestone road base 1987.
3. Uzan, J. "Characterization of granular material", Transp. Res. Rec. 1022, Transportation Research Board, Washington, D.C. 1985, pp. 52-59.
4. NCHRP “Laboratory determination of Resilient Modulus for flexible pavement design,” National Cooperative Highway Research Program (NCHRP) Project 1-28A. Transportation Research Board of National Academies 2004.
5. Nf EN-13286-7, Norme Européenne pour l’essai triaxial sous charge cyclique pour mélange sans liants hydraulique 2004.
6. Lekarp, F., Isacsson, U., Dawson, A., State of the art. I: Resilient response of unbound aggregates. Journal of Transportation Engineering / January/February 2000.
7. Heidarabadizadeh, N., Ghanizadeh, A.R., Behnood, A., Prediction of the resilient modulus of non-cohesive subgrade soils and unbound subbase materials using a hybrid support vector machine method and colliding bodies optimization algorithm. Construction and Building Materials 275, 122140 2021.

© 2022 London Journals Press

8. AASHTO “Guide for Design of Pavement Structures,” American Association of State Highway and Transportation Officials 1986.
9. Fall, M., Identification et caractérisation mécanique de graveleux latéritiques du Sénégal : application au domaine routier. Institut national polytechnique de lorraine Ecole Nationale Supérieure De Géologie De Nancy 1993.
10. Ki, B.I.J., Ba, M., Gueye, R., Hornych, P., Sana, A., Effect of Water Content and Grains Size Distribution on the Characteristic Resilient Young’s Modulus (Ec) Obtained Using Anisotropic Boyce Model on Gravelly Lateritic Soils from Tropical Africa (Burkina Faso and Senegal). Open Journal of Civil Engineering 11, 134–152 2021. https://doi.or g/10.4236/ojce. 2021.111009.
11. Bohi, Z.P.B., Caractérisation des sols latéritiques utilisés en construction routière : cas de la région de l’agneby (côté d’ivoire). L’école nationale des ponts et chaussées, France 2008.
12. Lawane Gana, A., Caractérisation des matériaux latéritiques indurés pour une meilleure utilisation dans l’habitat en Afrique L’Université du Havre et de la Fondation 2iE 2014.
13. Millogo, Y., Etude géotechnique, chimique et minéralogique de matières premières argileuse et latéritique du Burkina Faso améliorées aux liants hydrauliques : application au génie civil (bâtiment et route). Université de Ouaga 2008.
14. Samb, F., Modélisation par éléments finis des chaussées en graveleux latéritiques traités ou non et application au dimensionnement Mécanistique-Empirique Université De Thiès, Sénégal 2014.
15. Issiakou, M.S., Caractérisation et valorisation des matériaux latéritiques utilisés en construction routière au Niger Université de Bordeaux 2016.
16. El Abd, A., Développement d’une méthode de prédiction des déformations de surface des chaussées à assises non traitées (Thèse de doctorat). Université de Bordeaux I, 1970-2013, France 2006.
17. Ba, M., Comportement mécanique sous sollicitations cycliques de granulats quartzitiques de Bakel - Comparaison avec des matériaux de référence du Sénégal et d’Amérique (USA). Application au Dimensionnement Mécanistique-Empirique des chaussées souples. Université Cheikh Anta Diop de Dakar, Sénégal 2012.
18. Habiballah, T.E.M., Modélisation des déformations permanentes des graves non traitées. Université de limoges 2005.

© 2022 London Journals Press

This page is intentionally left blank

© 2022 London Journals Press

Scan to know paper details and
author's profile

Development of a New Profile of the Teeth of a Ginning Saw and its Results

Shukhratjon Imomkulov Bokijanovich & Muxtorova Iroda Kamoljon qizi

ABSTRACT

Currently, there is no scientific justification for improving the geometric parameters of the genie saw and the standards of accuracy of functional parameters. However, despite the success achieved in separating fiber from seeds during ginning, there are major disadvantages in that most cotton plants produce cotton fiber and seeds with increased ginning vices. The study on change of geometric parameters of various authors is considered. The issue of improving the geometrical parameters of the saw is important and therefore requires urgent resolution. The article discusses issues related to improving the profile of the teeth of the genie saw and increasing its productivity.

Keywords: improvement of the working surface, fiber size, fiber removal, brush drum, tooth thickness, fiber defects, fiber content.

Classification: DDC Code: 813.54 LCC Code: PS3553.L245

Language: English

London Journals Press

LJP Copyright ID: 392914
Print ISSN: 2631-8474
Online ISSN: 2631-8482

London Journal of Engineering Research

Volume 22 | Issue 5 | Compilation 1.0

© 2022. Shukhratjon Imomkulov Bokijanovich & Muxtorova Iroda Kamoljon qizi. This is a research/review paper, distributed under the terms of the Creative Commons Attribution-Noncom-mercial 4.0 Unported License http://creativecommons.org/licenses/by-nc/4.0/), permitting all noncommercial use, distribution, and reproduction in any medium, provided the original work is properly cited.

Development of a New Profile of the Teeth of a Ginning Saw and its Results

Shukhratjon Imomkulov Bokijanovich[α] & Muxtorova Iroda Kamoljon qizi[σ]

ABSTRACT

Currently, there is no scientific justification for improving the geometric parameters of the genie saw and the standards of accuracy of functional parameters. However, despite the success achieved in separating fiber from seeds during ginning, there are major disadvantages in that most cotton plants produce cotton fiber and seeds with increased ginning vices. The study on change of geometric parameters of various authors is considered. The issue of improving the geometrical parameters of the saw is important and therefore requires urgent resolution. The article discusses issues related to improving the profile of the teeth of the genie saw and increasing its productivity.

Keywords: improvement of the working surface, fiber size, fiber removal, brush drum, tooth thickness, fiber defects, fiber content.

Author α: Associate professor of the department "General technical disciplines", Namangan engineering and technology institute, Uzbekistan, Namangan.
σ: Senior Lecturer of the Department "General Technical Disciplines", Namangan engineering and technology institute, Uzbekistan, Namangan.

I. INTRODUCTION

Since the most ancient times, people have used cotton mainly after separating the fiber from its seeds. Initially, the separation of cotton fibers from seeds was carried out manually. At the same time, the productivity of one person did not exceed 1 kg per day [1].

The development of the history of mankind has led to the fact that the separation of cotton fiber from seeds has been carried out by machine.
Especially in such areas, the achievement of science is the improvement of the main working bodies of the profile of the laser saw [2].

Taking into account the prevailing influence of the state of the teeth of the saw blade on the quality of processed raw cotton products, it is necessary to ensure high-quality production of the disk in compliance with both the geometric parameters of the tooth and the roughness of its working surfaces.

The articles of E. A. Normatov [3] and A. A. Ismailov et al. [2] were published on the change in the geometric parameters of the tooth.

In both articles, the questions of the geometry of the saw tooth were considered in more detail and the following conclusions were made:

Akhmedova S. came to the conclusion that " With a shorter tooth with a constant pitch and a cavity having the most rational shape, i.e. the shape of an isosceles triangle with the largest gripping area, the gripping ability does not decrease, and the tooth becomes more stable and more economical in operation. Based on this, you can find the height."

According to Normatov E. A., the tooth height is equal to 2.6 mm [3].

Ismailova A. A. and others on the basis of theoretical research came to the following main conclusions:

The maximum value of the fiber capture area will be at the angle: $\alpha = 90^o - \gamma$;

where: γ is the angle between the guides of the relative speed of the fiber and the circumferential speed of the saw. Note that the article does not address issues related to the height of the tooth and does not draw appropriate conclusions, it is not agreed with the statement of the authors, we note that to the angle α=45°, the corresponding height of the tooth is h=2.6 mm (at r=0.4 mm and the angle of sharpening δ=20°) [4].

© 2022 London Journals Press

Makhkamov R. G., based on the analysis of the literature [3], as well as on the basis of his previous theoretical assumptions, considers the issue of the geometry of the tooth of a chain saw and makes the following proposals: Reduce the height of the saw teeth to 2.6 mm; keep the gap between the grates within 2.8–3.2 mm; the tooth chamfer should be removed.

However, despite the success achieved in separating fiber from seeds during ginning, there are major disadvantages, they are that most cotton mills produce cotton fiber and seeds with increased ginning defects.

In order to determine the optimal variants of the profile of the teeth of the laser saw, a laboratory installation was tested. The optimal profile of the saw tooth was determined, aimed at reducing its height. Then the teeth with such profiles were tested in production jeans and some results were obtained to reduce the amount of fiber defects and seed crushing.

When analyzing the results of ginning and with the same tooth profiles on the laboratory and production gin, we found some changes.

For example, when ginning "VL-10", intense cotton motes occurred with a long tooth, and when testing saw blades with a height of 2 mm on a production gin, the opposite results were obtained, i.e. intense cotton motes occurred with a short tooth [7].

II. EXPERIMENTAL PROCEDURES

E. A. Normatov, on the basis of logical assumptions, considered the work of the tooth in relation to the work of the grate, the raw chamber and the brush drum. The author did not consider the issues of tooth geometry.

He [4], in the article "Points of ginning saws", also considered the geometry of the tooth of a gin saw; " ... the slope of the back of the top of the tooth is not needed today, and the saw tooth can have a trapezoidal shape with a flat top, rather than a triangular one ...". The author proposed to obtain such a flat top at a point due to a slight shortening of the tooth height. In conclusion, the author suggests that the proposed method allows for the possibility of repeated tooth points, since the analysis of its operation proves that the working face of the tooth, i.e. the face, which is really necessary for work and gives products, does not exceed 3/3 of its entire height, therefore, there is no danger of deterioration in productivity, even if the saw tooth is worn off and ½ of its height."

In the collection No. 4 of the Pilot Plant, an article was published by U.A. Sapaev, "Evaluation of the use of various devices for ginning wet snapper", in which an attempt was made to install a stirrer in the raw gin chamber to ensure normal rotation of the raw roller when ginning cotton from a wet snapper. The author came to the conclusion that the use of agitators does not provide significant assistance. Therefore, they have not found application in industry.

During the same period, a researcher at Central Research Institute of the Cotton Industry (CRICI) Tilabov B. N. studied the influence of the quality of steel used for the production of saws and the properties of raw cotton on the service life of saws in the work "The influence of hardness and strength of steel on the main indicators of ginning". As a result of the research, the author came to the conclusion that the service life of the saw cylinder is determined not by the wear resistance of the saw steel, but solely by the amount of foreign impurities that got into the working chamber of the gin, the size of the tooth and the mechanical qualities of the steel from which the saw is made.

In 1989, No. 5 of the Textile Industry magazine published an article by Gulidov N. G. "On the profile of the tooth of a genie saw", in which the idea is expressed about determining the rational profile of the tooth, according to which an increase in the angle α (front face) should be accompanied by a decrease in the height of the tooth.

According to Gulidov's proposal, the angle α and the height h should mean that an increase in the angle α (the front face) corresponds to a decrease in the height of the tooth (the other parameters do not change).

© 2022 London Journals Press

In 2008, an article by R. G. Makhkamov "On the theory of fiber separation" was published, which deals with the issues of deducing the shape of the tooth of the parabolic form of its anterior face, the author wrote "Based on the optimal conditions of tooth strength to increase its gripping ability by increasing the angle of inclination of the working face, we build a parabola with a vertex at the base of the working face of the tooth".

Note that a tooth with a parabolic construction of the front face has not found application in industry due to the complexity of its manufacture.

This contradiction is explained by the design features of the laboratory and production gins, that is, the first fiber is removed by a brush drum, and the second by an air-removing device. There are also differences in power, speed, working bodies, and much more [5].

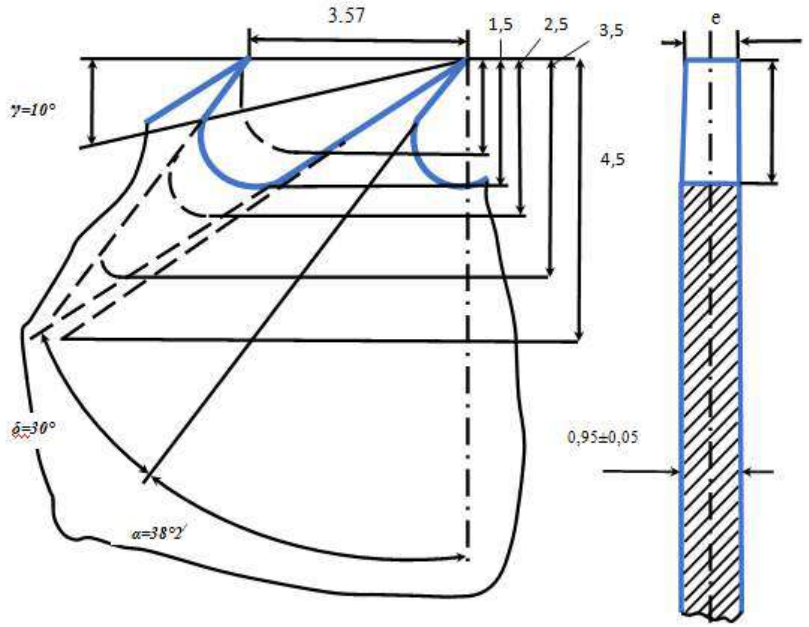

Fig. 1: Schemes of the tooth of a chain saw with different thickness at the top

e-I option-saw blades had teeth of thickness at the top = 0.2-0.3 mm, i.e. on both sides of the tooth, the chamfer was removed on abrasives

This was the objective reason that forced us to conduct further experiments only in production conditions - on existing gins.

Further, on the basis of experiments conducted only on production gins, the issues of the influence of different tooth heights of a genie saw on the technological properties and on the nature of ginning are highlighted.

Experiments of some factories have shown that the work of teeth with an increased thickness of the tooth tip against GOST 1413-48 gave some improvements in product quality. In this regard, the first task was to determine the thickness of the tooth at the top, and then to determine the rational height of the tooth.

When determining the optimal thickness of the top of the saw tooth, the remaining parameters of the tooth remained in accordance with GOST 1413-48.

The peculiarity of our tests was to conduct them in production conditions.

Saw blades with a diameter of 312 mm with different thicknesses at the tops of the teeth were prepared in five versions of 100 saws each (Fig. 1).

Option II - at e= 0.4-0.5 mm, the chamfer is removed from both sides of the tooth.

Option III - at e= 0.6-0.7 mm, the chamfer is slightly removed from both sides of the tooth.

© 2022 London Journals Press

Option IV - at e= 0.8-0.9 mm, only the burrs were removed from the exit side of the punch.

V option - at 0.95 > e > 0.9, i.e. the teeth after the intersection were not processed for chamfering or burr removal, only grinding was carried out in sand baths according to the existing operating instructions of the saw shop equipment.

The saw blades of the I-IV variants were also subjected to grinding under different conditions, in a sand bath according to the existing instructions.

The saw blades of each variant were separately mounted on certain shafts for a separate battery genie. Thus, each gin was completed with saws of a certain variant, after which all gins underwent the same adjustment.

The tests were carried out under the same conditions and different ginning modes. All gins worked mainly on the fourth tooth of the power supply, which corresponded to a productivity of 9-10 kg of fiber per saw per hour. The pressure in the air chamber was maintained equal to 180-140 water column. The duration of the test on the II, III and IV variants was 48 hours, on the I and V variants 4 hours. The reason for the short duration of the I and V variants was a noticeable deterioration in the quality of fiber and seeds due to an increase in the density of the raw roller and poor removal of fiber from the teeth, especially in the V variant. In the II, III and IV variants, the ginning process proceeded normally and the fiber was also eaten normally.

Further research was carried out at sawmills of cotton gins.

The object of the test work was laser saws of various shapes and parameters. The tests were carried out in 3 stages.

At the first stage of research work, saws were installed on the sewing machines according to the PDI 64-2016 standards, and during one shift, the operation of the machine and the quality indicators of the products were monitored. The obtained data are summarized in a table.

At the second stage of the study, the object of the study was 5 types with different thickness of the tooth tip ("e"): 0,2-0,3; 0,4-0,5; 0,6-0,7; Laser saws of 0.8-0.9 and 0.95 ± 0.05 mm were obtained. The remaining parameters of the pil gin were adopted in accordance with the current PDI 64-2016 guidelines.

The different height in the third direction was achieved by changing the angle of penetration of the tooth, the radius of the tooth was 0.4 mm, and the difference in the height of the tooth in the third direction was associated with a change in the angle of penetration of the tooth. the radius of the tooth (in all variants, the cutting angle was about 20°).

In all variants, the thickness of the tooth tip was 0.8 ± 0.1 mm, the tooth pitch was 3.57 mm, the disc diameter was 312 mm, the tooth thickness was 0.95 ± 0.05 mm. As a result, 1 in the first line; 1,5 ± 0,2; 2,5; 3,5; 4.5, 1.5 on the second line; 2.0 ± 0.1; 2.5; 3.5; Divided into teeth with a height of 4.5. From saws with such teeth, saw cylinders were made in the current order, placed in a denim machine and the cleaning process was carried out.

In the initial test, the quality of cotton fiber obtained with a tooth tip thickness of 0.8 ± 0.1 mm, a tooth height of 1.5 ± 0.2 and 2.0 ± 0.1, and a tooth rounding radius of 0.6-0.8 mm, showed that they changed for the better. The results confirmed that the direction of the study was chosen correctly.

The third chapter of the dissertation, entitled "Fundamentals of the design of the teeth of the gin saw", is devoted to the parameters of the saw, which is the main working organ of the gin saw, and its teeth. In fact, the main working surface of the saw is the tooth profile. The geometric parameters of the tooth profile determine the efficiency of the saw, that is, increasing the service life of the saw teeth, improving the quality and quantity of cotton products largely depend on the parameters of the saw teeth.

While the main parameters of the saw blade are its diameter, thickness and number of teeth, the main geometric parameters of the tooth profile are its height, pitch, angle of the front blade, the

© 2022 London Journals Press

radius of rounding of the sub-tooth and the thickness of the tooth.

Changes in the geometric parameters of the teeth of the saw blade significantly affect the speed of the roller of the initial material of the saw blade and the composition of the cotton layer on its periphery, the size of the arc in contact with the saw blade, and the distance of penetration of the saw blade inside. untreated roller. Therefore, the height of the tooth has long been the subject of study of scientific and production personnel.

As a result of theoretical and practical studies of pil gin, equations were obtained for determining the optimal geometric parameters of pil gin.The theoretical height of the tooth can be determined from the following equation:

$$h = \frac{t \cdot \sin\gamma \cdot \cos\alpha}{\cos(\alpha+\gamma)}$$

where: γ is the angle of inclination of the leading edge of the saw;
α - angle of inclination of the rear edge of the saw;
t-tooth pitch

A graphical analysis of the obtained equation showed that the most active factor affecting the height of the tooth is the distance between the teeth. As the tooth pitch increases, the tooth height increases linearly. As the slope of the front edge of the tooth increases, the height of the tooth increases, decreasing with decreasing. The angle of inclination of the posterior edge of the tooth, on the contrary, negatively affects the height of the tooth, i.e. its increase leads to a decrease in the height of the tooth.

Experimental studies on the justification of dental parameters were carried out on a 30-caliber denim device in the scientific laboratory of the Namangan Institute of Engineering and Technology. To facilitate the experiments, one factor was selected for each experiment. In the first experiment, the effect of the height of the saw tooth on the mass fraction of impurities and defects in the fiber was studied. An empirical equation of the following form was chosen for the study:

$$y = ax + b_0$$

where: a is the angular coefficient of the straight line;

x is the height of the gin saw tooth;
b is the section of a straight line from the ordinate axis

Based on the results of the experiment, we determine the value of the parameters "a" and "b" in the equation by the least squares method from the following equation:

$$a = \frac{n\sum x_i y_i - \sum x_i \sum y_i}{n\sum x_i^2 - \left(\sum x_i\right)^2} = 0{,}181$$

$$b = \frac{n\sum x_i y_i - \sum x_i \sum y_i}{n\sum x_i^2 - \left(\sum x_i\right)^2} = 2{,}41$$

where: n is the number of variants of the condition being checked, that is, 5.

Thus, the empirical equation that we are looking for is the relationship between the mass fraction of impurities and defective impurities in the fiber " y "and the height of the tooth "x" of the gin saw:

$$y = 0,181x + 2,41$$

In the same way, the effect of the height of the saw teeth on the mechanical damage of cotton seeds was studied. The empirical equation obtained as a result of the study represents the effect of mechanical damage to a tooth with a height of "x" on mechanical damage to "y":

$$y = 0,0696\ x + 0,3589\ ,$$

III. RESULT AND DISCUSSION

To assess the technological properties of fiber and seeds, the plant's laboratories were sampled under our control and according to the developed methodology [10].

Fiber samples were taken from the neck of each gin for each variant, seed samples from the seed trays of each gin. The sample was taken three times per shift, i.e. for the II, III and IV variants 18 times, and for I and V-3 times.

© 2022 London Journals Press

Technological analyses were carried out in the laboratory of the plant according to the existing rules.

At the time of sampling, the current strength in the phases of the electric motor of the gin saw cylinder was also measured.

For clarity, the results are presented in the form of graphs 1-3.

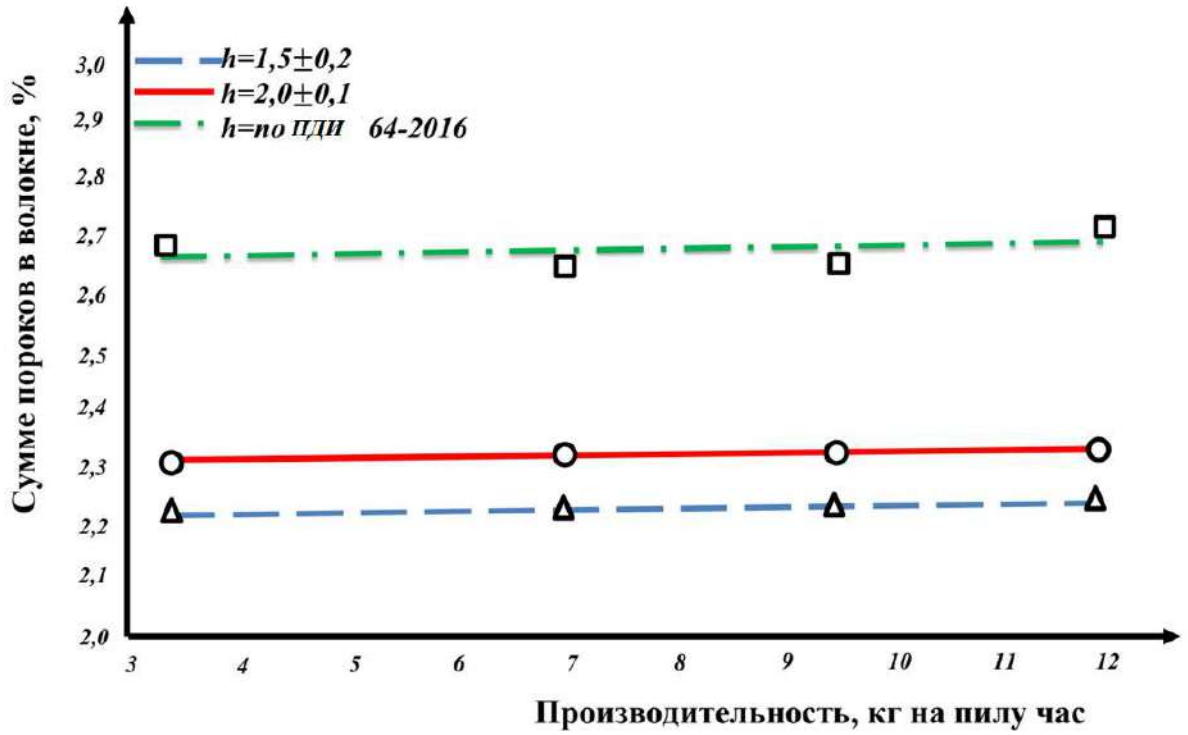

Graph 1: The dependence of the amount of fiber defects on the effectiveness of gin

From Graph 1, it can be seen that with an increase in the thickness of the tooth vertices, the amount of defects in the fiber decreases, which occurred mainly due to a decrease in broken seeds in the fiber. At the same time, the content of litter and motes in the fiber almost does not change.

The explanation that an increase in the thickness at the top of the tooth causes a decrease in the amount of defects in the fiber, apparently, is that the specific pressure of the tooth edge on the fiber and seeds decreases and this was accompanied by a decrease in the damage of the latter.

In contrast to the general pattern, the sum of fiber defects on the V variant of saws had an overestimated value.

This can be explained by the fact that the saw blades of the V variant after the tooth crossing did not undergo chamfering, only the teeth were ground in a sand bath under different conditions with other options for preparing saws. Apparently, such an identical condition for processing teeth for all variants is insufficient for the V variant and the teeth of the V variant, obviously, have not been freed from invisible burrs. Thus, the number of burrs on the teeth of the V variant was greater than on the teeth of the I, IV variants. And in the industry, it has long been known that the presence of burrs leads to a deterioration in the quality of products.

© 2022 London Journals Press

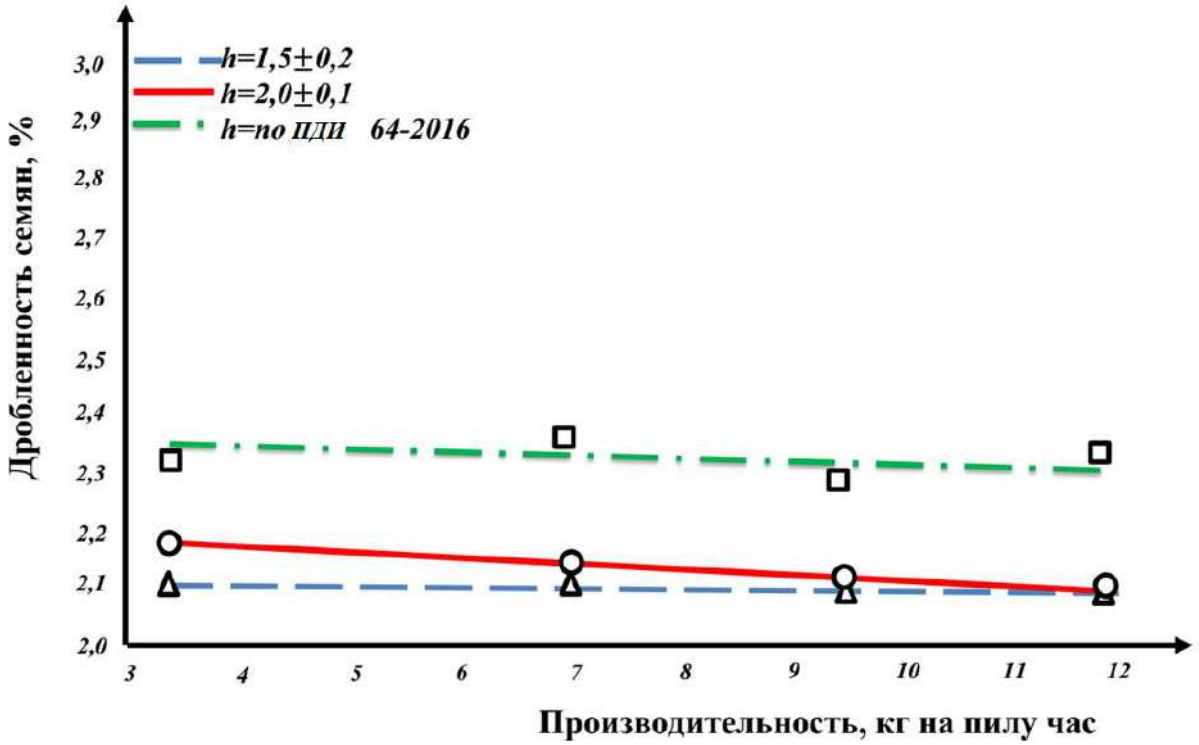

Graph 2: The dependence of mechanical damage to seeds on the effectiveness of gin

Graph 2 shows that the change in the crushing of seeds is inversely proportional to the change in thickness at the vertices of the tooth. The reasons for this can also be found in the change in the specific pressure on the seeds from the edge of the tooth.

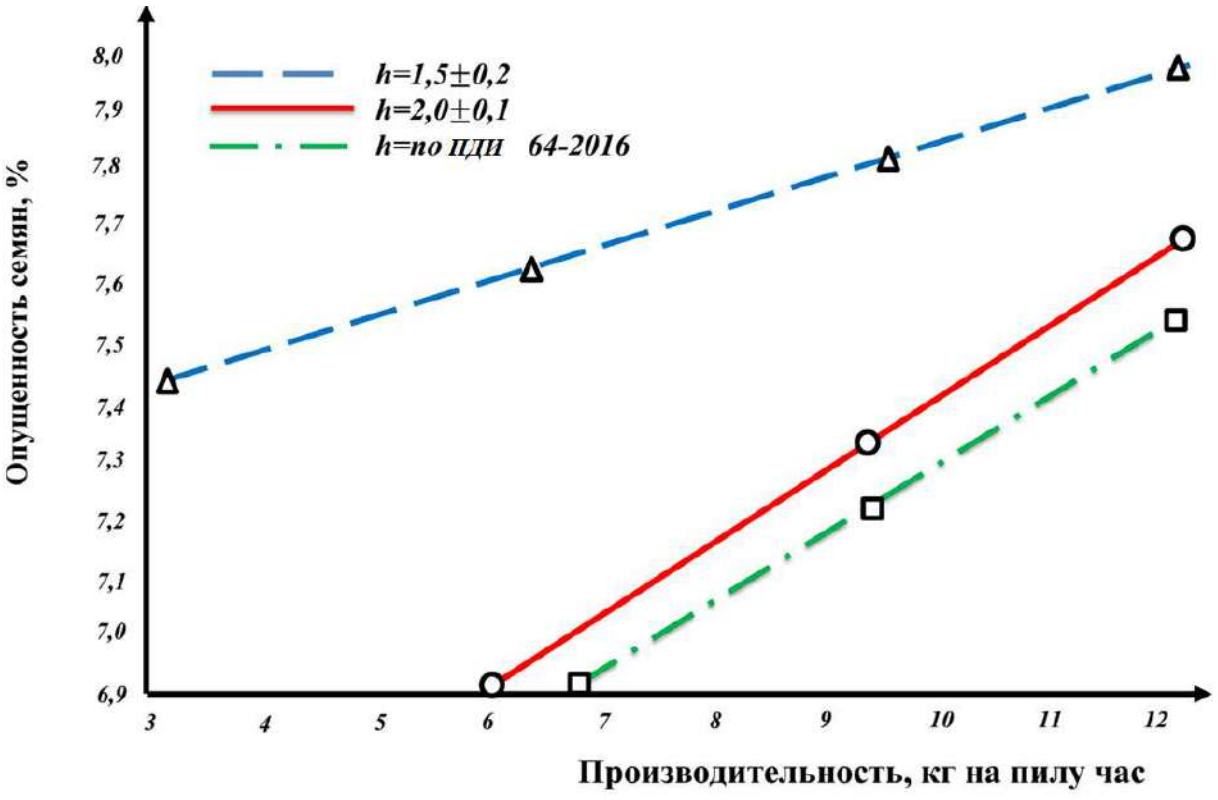

Graph 3: Dependence of seed pubescence on the effectiveness of gin

© 2022 London Journals Press

It can be seen from Graph 3 that the change in the total omission of seeds occurs in the opposite proportion to the change in the thickness of the top of the tooth.

IV. CONCLUSION

It is possible that partial linterization processes also occur during the ginning process. If we assume this, then in our case, an increase in the thickness at the top of the tooth also caused an intensification of the linterization process during ginning. Therefore, an increase in the thickness at the top of the tooth caused a decrease in the complete omission of seeds.

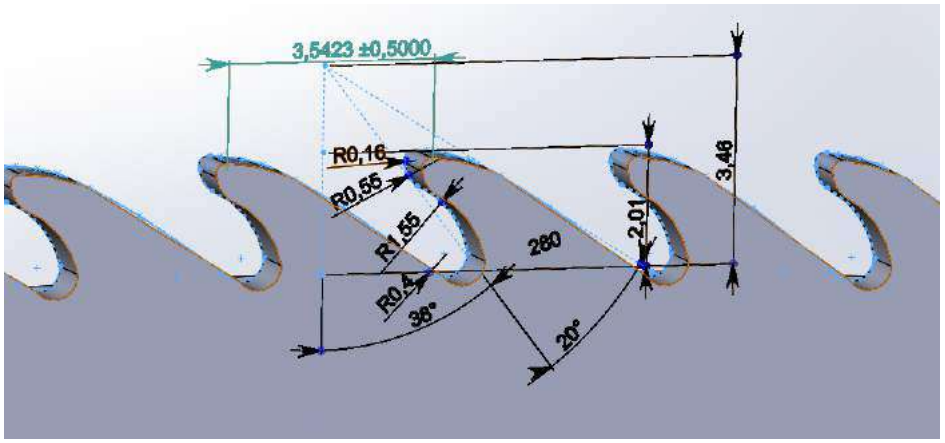

Fig. 2: The developed profile of the tooth of the genie saw

It can be seen from Graph 4 that the residual fiber content of the seeds changes in inverse proportion to the change in the thickness of the tooth tip. The explanation for this is the same as in Graph 3.

And, finally, it can be seen from Graph 5 that the law of changing the load on the electric motor of the gin saw cylinder with respect to the change in tooth thickness proceeds according to the law of direct proportion.

The explanation of the latter is that with an increase in the thickness at the top of the tooth, the degree of its contact with the mass of the raw roller increases and this causes an increase in the load on the gin shaft.

Thus, according to the results of the test, we come to the conclusion that the rational thickness at the top of the saw tooth is equal to e = 0.8 ± 0.1 mm, at which it is possible to obtain products of the proper quality.

REFERENCES

1. Sapaev. U. A. Evaluation of the use of various devices when ginning a wet snapper. "Problems of textiles" Tashkent, 2009, No. 2. pp. 51-56.
2. E. A. Normatov, A. A. Ismailov, U. A. Sapaev, "Theoretical study of the oscillation frequency of the gin grate". Collection of the scientific and practical conference. Namangan 2011, 2-volume, pp. 303-305.
3. E. A. Normatov, A. A. Ismailov, "Methods of increasing the durability of diamond saws and grates". Collection of materials of the republican scientific and practical conference of young scientists. Tashkent, 2011, pp. 71-73.
4. A. A. Ismailov, A.M. Akhmedov, A. A. Safoev, E. A. Normatov. "Improvement of the grate and the teeth of the genie saw" Collection of materials of the republican scientific and practical conference of young scientists. Tashkent, 2011, pp. 27-30.
5. E. A. Normatov, A. A. Ismailov, A.M. Akhmedov, U. A. Sapaev ," Study of the wear resistance of various materials of laser saws " Collection of materials of the republican scientific and practical conference of young scientists. Tashkent, 2010, pp. 119-121.

© 2022 London Journals Press